Molecular Neurobiology (2021) 58:5031–5051
https://doi.org/10.1007/s12035-021-02478-8

Noopept Attenuates Diabetes-Mediated Neuropathic Pain and Oxidative Hippocampal Neurotoxicity via Inhibition of TRPV1 Channel in Rats

Halil Düzova[1] · Mustafa Nazıroğlu[2,3,4] · Bilal Çiğ[5] · Perihan Gürbüz[6] · Ayşe Nur Akatlı[7]

Received: 28 April 2021 / Accepted: 27 June 2021 / Published online: 9 July 2021

Abstract

Neuropathic pain and oxidative neurotoxicity are two adverse main actions of diabetes mellitus (DM). The expression levels of calcium ion (Ca^{2+}) permeable TRPV1 channels are high in the dorsal root ganglion (DRGs) and hippocampus (HIPPO). TRPV1 is activated by capsaicin and reactive free oxygen radicals (fROS) to mediate peripheral neuropathy and neurotoxicity. Noopept (NP) acted several protective antioxidant actions against oxidative neurotoxicity. As DM is known to increase the levels of fROS, the protective roles of antioxidant NP were evaluated on the DM-mediated neurotoxicity and neuropathic pain via the modulation of TRPV1 in rats. Thirty-six rats were equally divided into control, NP, DM (streptozotocin, STZ), and STZ + NP groups. A decrease on the STZ-mediated increase of neuropathic pain (via the analyses of Von Frey and hot plate) and blood glucose level was observed by the treatment of NP. A protective role of NP via downregulation of TRPV1 activity on the STZ-induced increase of apoptosis, mitochondrial fROS, lipid peroxidation, caspase -3 (CASP-3), caspase -9 (CASP-9), TRPV1 current density, glutathione (GSH), cytosolic free Zn^{2+}, and Ca^{2+} concentrations in the DRGs and HIPPO was also observed. The STZ-mediated decrease of glutathione peroxidase, GSH, vitamin E, and β-carotene concentrations in the brain cortex, erythrocyte, liver, kidney, and plasma was also attenuated by the treatment of NP. The STZ-mediated increase of TRPV1, CASP-3, and CASP-9 expressions was decreased in the DRGs and HIPPO by the treatment of NP. In conclusion, the treatment of NP induced protective effects against STZ-induced adverse peripheral pain and HIPPO oxidative neurotoxicity. These effects might attribute to the potent antioxidant property of NP.

Keywords Apoptosis · Diabetes · Neuropathic pain · Noopept · Oxidative stress · TRPV1 channel

✉ Mustafa Nazıroğlu
mustafanaziroglu@sdu.edu.tr

[1] Department of Physiology, Faculty of Medicine, Inonu University, Malatya, Turkey

[2] Neuroscience Research Center, Suleyman Demirel University, Isparta, Turkey

[3] Drug Discovery Unit, BSN Health, Analyses, Innovation, Consultancy, Organization, Agriculture, and Industry Ltd., Isparta, Turkey

[4] Department of Biophysics, Faculty of Medicine, Suleyman Demirel University, Isparta, Turkey

[5] Department of Physiology, Faculty of Medicine, Ahi Evran University, Kırşehir, Turkey

[6] Vocational School of Health Services, Inonu University, Malatya, Turkey

[7] Department of Pathology, Faculty of Medicine, Inonu University, Malatya, Turkey

List of Abbreviations

DM	Diabetes mellitus
DNP	Diabetic neuropathy
DRGs	Dorsal root ganglions
HIPPO	Hippocampus
Int-fROS	Intracellular fROS
NP	Noopept
fROS	Free reactive oxygen radicals
STZ	Streptozotocin
TRPV1	Transient receptor vanilloid 1
mPTP	Mitochondrial permeability transition pore

Introduction

Diabetes mellitus (DM), as a prevalent chronic disease, has an increasing incidence rate over the world [1]. The treatment deficiencies and late diagnosis of DM generally lead the life quality decreasing complications [2]. A main chronic

complication of DM is diabetic neuropathy (DNP) [3]. DNP is mainly caused by the functional and structural disorders mediated by metabolic and vascular changes, which are related to oxidative stress-induced neurotoxicity in neuronal tissues, including hippocampus (HIPPO) and dorsal root ganglion (DRGs) [4–6]. One of the important factors leading to oxidative stress enhancement is the increase of intracellular Ca^{2+} input in the hyperglycemia and free reactive oxygen radicals (fROS) generation with mitochondrial activity [7, 8]. In addition, it has been determined that an increase of regional Ca^{2+} concentration in the damaged area or spinal canal is a cause of neuropathic pain [9]. Non-steroidal anti-inflammatory and opiate drugs are used in chronic pain management approaches [10]. However, there is no effective accepted protocol in the treatment of DNP due to the insufficiency and high side effect profile of the mentioned drugs. Therefore, intensive research is carried out on the pathogenesis and treatment of DNP.

Na^+ and Ca^{2+} permeable-voltage gated ion channels have physiological impact on insulin secretion and DNP pathogenesis [11]. The nociceptors (Aδ and C fibers) in the dorsal root nuclei are target cells of painful DNP [12]. Also, diabetes-mediated changes in the neuronal Ca^{2+} homeostasis and antioxidant redox system have been detected in the oxidative injury of the HIPPO [6, 13]. Transient receptor potential (TRP) family channels mostly affect non-selective ion channels, which are simultaneously permeable to Na^+ and Ca^{2+} [14, 15]. A member of the TRP superfamily is the TRP vanilloid 1 (TRPV1) channel. The main activators of TRPV1 are high temperature, acidic pH, vanilloids, oxidative stress, and hot chili component (capsaicin, CAP) [16–18]. One of the TRPV1 antagonists is AMG 9810 (AMG) [19]. The antagonist action of AMG was reported in the DRGs and HIPPO [20, 21]. In the DM, the oxidative stress-mediated increase of Ca^{2+} input through TRPV1 channel into the DRGs and HIPPO plays an important role in the induction of DPN [13–15]. Studies have shown that the expression levels of TRPV1 are widespread in the nervous system, including DRGs and HIPPO [22, 23]. These channels have been determined to be responsible for pain transmission in sensory neurons, including DRG, and in the damage of some areas of the brain, including the HIPPO [13–15, 22]. In the TRPV1 studies, an increase in the intracellular free Ca^{2+} ($[Ca^{2+}]_i$) concentration which is known to have role in the pathogenesis of DN has been observed to the cause of mitochondrial fROS generation, apoptotic cell damage, and oxidative neurotoxicity [13, 20, 21]. Neuroprotective actions of antioxidants such as melatonin and selenium against diabetes-mediated HIPPO and DRGs oxidative neurotoxicity via inhibition of TRPV1 were recently reported [13]. However, the neuroprotective effect of antioxidant Noopept (NP) (GVS-111, N-phenylacetyl-L-prolylglycineethyl ester) against DM-mediated HIPPO and DRGs oxidative neurotoxicity via inhibition of TRPV1 has not been clarified yet.

The NP is a synthetic nootropic dipeptide produced from the nonpeptide prototype of vasopressin and piracetam [24–26]. The molecular action mechanism of piracetam and similar drugs are still not fully revealed, although they have been shown to regulate the excitatory and/or inhibitory effects of the neurotransmitter, neurohormone, oxidative stress, and neurotransmitter signals in the brain [27, 28]. At the cellular level, NP blocks voltage-dependent calcium and calcium-dependent potassium channels [29–31]. Also, NP has been determined to facilitate synaptic transmission in the HIPPO, reduce the neurotoxic effects of glutamate in neuron culture, reduce fROS and apoptosis, and reduce oxidative stress and strengthen antioxidant system activity [26, 32, 33]. Also, NP has been found to exhibit protective activity in the mitochondria by preventing mitochondrial cyclosporin-A channels opening and restoring the mitochondrial transmembrane potential [26]. Furthermore, NP has been shown to have positive effects on blood glucose levels, body weight changes, and pain sensitivity in researches with streptozotocin (STZ)-induced DM model [34, 35], although its possible mechanism on the DNP in rats has not been clarified yet.

In the current study, we investigated the protective action of NP treatment on the TRPV1-mediated DNP and oxidative neurotoxicity in the DRGs and HIPPO of rats with DM.

Material and Methods

Animals

In the current study, the study was started by using 40 male Wistar Albino rats (aged 12 weeks old). The animals were housed in the Experimental Animal Research Center of Suleyman Demirel University (SDU) under controlled-laboratory conditions (temperature: 21 ± 2 °C, humidity: 65% rooms and a 12:12 h light–dark cycle). The animals were freely accessed to the water and food. The intraperitoneal (i.p.) injections of NP and STZ to the rats were performed at mornings (between 08.00 and 09.00).

Ethical Approves

The study was approved by the Experimental Animal Research Center of SDU (Permit Number: 2019–06-03) and Inonu University (Permit Number: 2017/A-13), because the study was performed in SDU and Inonu University. All analyses in the current study were generated in BSN Health, Analysis and Innovation Ltd. Inc. Teknokent, Isparta, Turkey.

Study Groups of Rats

The study was started with 40 rats. Rats were randomly divided into randomized 4 groups as control (Ctr), NP, STZ, and STZ + NP. After the STZ injection, 4 rats of STZ groups died within 3 days. Finally, the experiment ended with nine ($n = 9$) rats in Ctr, STZ, and STZ + NP groups:

Ctr group: After waiting 14 days, daily i.p. 10 µl DMSO and 990 µl physiologic saline were administered to the rats in the Ctr groups for 28 days.
NP group: After waiting 14 days, the dose of NP (5 mg) dissolved in 100-µl dimethylsulfoxide (DMSO) and its 10 µl was diluted with 990 µl physiologic saline (0.9%). The diluted NP as 0.5 mg/kg body weight was i.p. administered once daily for 28 days [25].
STZ group: For induction of type I DM in the rats, 55 mg/kg (dissolved in sodium citrate buffer with pH 4.5) of STZ (Sigma-Aldrich) was freshly administered i.p. in a single dose after 12 h fasting [36]. After 3 days of the first STZ injection, the blood glucose levels were measured using an eBsensor glucometer (Visgener Inc., Hsinchu City, Taiwan). Animals with high (≥ 250 mg/dl) fasting blood glucose levels were used in the STZ group. Then, the diabetic rats were kept 14 days in the cages without NP treatment for the induction of neuropathic pain. The presence of neuropathic pain was tested by Von Frey and Hot plate tests as explained below. Then, the rats in the group were further kept in the cages for 28 days.
STZ + NP group: Diabetes were induced rats by the STZ treatment as described in a previous study [36]. Then, the rats with DM were kept 14 days in the cages without NP treatment for the induction of neuropathic pain. After confirming the neuropathic pain at 14 days by Von Frey and hot plate tests, the NP (0.5 mg/kg body weight) was dissolved in 10 µl DMSO and 990 µl physiological saline (0.9%) and then the dose of NP for each rat was administered i.p. once daily for 28 days [25].

At the 42nd day of the experiment, all animals were sacrificed by taking blood from their hearts after the anesthesia (70 mg/kg ketamine and 8 mg/kg xylazine). Then, the DRGs, HIPPO, brain cortex, blood, liver, and kidney samples were obtained from the rats.

Blood Glucose Measurements and Hyperalgesia Tests in the Rats

The fasting blood glucose analyses of tail blood (via glucometer, eBsensor model) and the hyperalgesia tests of paw (via Von Frey and hot plate) were performed between 10:00 and 11:00 a.m. at baseline, 7th, 14th, 21st, 28th, 35th, and 42nd days in the Ctr, NP, STZ, and STZ + NP groups. The analyses of mechanical hyperalgesia were measured by using the calibrated von Frey monofilaments (20PC Aesthe, Muromachi Kikai Ltd. Tokyo, Japan) as described in a previous study [37]. The method of Von Frey was applied with increasing force until a withdrawal response. After observing the response, the force of the von Frey filament was accepted as mechanical withdrawal threshold. The evaluation of thermal nociceptive threshold in the animal of each group was performed by hot plate test [37].

The Preparations of HIPPO and DRGs Samples

The skull of rat was properly opened. The samples of HIPPO were obtained from the brain. The neurons of DRGs between L4 and L5 regions were separated from the lumbar area of rats. The whole DRGs within lumbar bone were used for the obtaining laser confocal microscope (LSM) image (LSM800, Zeiss, Ankara, Turkey). For the spectrofluorometer (Fura-2) and plate reader analyses, the attached nerves and surrounding connective tissues of DRGs and HIPPO were removed, and they were exposed to the further procedures as described in previous studies [8, 9, 13]. Briefly, the DRGs and HIPPO after taking were exposed to trypsin type III enzyme and 0.5 mg/ml type XI collagenase (Sigma-Aldrich) in 5-ml DMEM medium at 37 °C in a shaking bath for 45 min. The enzymatic digestion was stopped by using the soybean trypsin inhibitor (1.25 mg/ml, type II-S1, Sigma). After dissociation with a sterile syringe and centrifugation at 1500 g, the DMEM medium was removed, and the neurons were seeded on the sterile 25 T flasks with filter caps (1×10^6 neurons). The DRG and HIPPO were cultured in the DMEM-LPXA with low glucose (1 g/l), because the high glucose in the cell culture medium induces TRPV1 activation in neuronal cells [38].

Determination of $[Ca^{2+}]_i$ Concentration in the Neurons of DRG and HIPPO by Using Fura-2

For the $[Ca^{2+}]_i$ concentration analyses in the DRGs and HIPPO, a Carry Eclipse spectrofluorometer (Varian Inc, Sydney, Australia) was used, and details of the analyses were described in previous studies [8, 9, 13, 37]. The neurons of DRG and HIPPO were loaded with 4 µM fura 2AM-acetomethoxy ester (Molecular Probes) for 45 min at 37 °C. Then the fluorescence changes were recorded at 510 nm by using the Varian spectrofluorometer with 1-s intervals after excitations (340 and 380 nm). The $[Ca^{2+}]_i$ concentration is indicated as nanomolar (nM) taking a sample every second [13, 37].

Electrophysiology in the DRGs

The patch-clamp records at whole cell configuration were recorded in a HEKA EPC 10 amplifier (Lamprecht, Germany) by using Patch-master software. Voltage-clamp configuration at − 65 mV was induced and currents were recorded. The content details of intracellular and extracellular buffers were indicated in previous studies [8, 9, 13]. In addition to the AMG, the currents of TRPV1 were blocked by using Na^+ free patch chamber solution (*N*-methyl-D-glucamine, $NMDG^+$). Patch pipettes with 4 ± 2 MΩ resistances were produced in a P-97 puller (Sutter Instrument Lab, Ankara, Turkey) from borosilicate glass pipettes. The DRGs were activated with CAP (10 μM) for the stimulation of TRPV1 or AMG 9810 (10 μM) for the inhibition of TRPV1. The current results of TRPV1 results were expressed as the current density (pA/pF). The adult HIPPO neurons are too small according to the tip diameter (2–5 μm) of patch pipettes. Hence, the patch clamp analyses were not able to perform in the HIPPO neurons.

Laser Confocal Microscope (LSM) Analyses: the Fluorescence Intensity Analyses of $[Ca^{2+}]_i$ Concentration (Fluo-3AM), Death Cell Rate, Mitochondrial Membrane Potential (ΔΨm, MMP), Intracellular fROS (Int-fROS), Mitochondrial fROS (Mito-fROS), Intracellular Free Zn^{2+}, and Intracellular Glutathione (GSH) Levels

We assayed STZ-mediated fluorescence intensity changes of $[Ca^{2+}]_i$ in the DRGs in the LSM 800 by using 1 μM Fluo-3AM (Calbiochem GmbH, Darmstadt, Germany) incubation previously described [37].

The stain of Hoechst 33342 can easily pass into the nucleus of live cells, and its blue color indicates live cell number. However, the stain of propidium iodide (PI) represents red color because it can only permeable into the nucleus of injured cells. The DRGs in the dishes with glass bottom were incubated with the combination of PI (2 μg/ml) and Hoechst 33342 (5 μM) (Cell Signaling Technology, Istanbul, Turkey) before the LSM800 analyses [37].

The accumulation of JC-1 stain increases in the mitochondria according to increase of mitochondrial membrane potential (ΔΨm, MMP) level [38, 39]. The membrane potential changes (ΔΨm) in the mitochondria were assayed by the incubation of 3 μM JC-1 stain (Cayman Chemical Inc. Ann Arbor, Michigan, USA) [37].

The generation of Int-fROS was analyzed in the LSM800 microscope by using 2′,7′-dichlorofluorescin diacetate (DCFH-DA) and DHR123 non-fluorescent stains. The DCFH-DA is oxidized to a fluorescent intracellular, (2', 7' -dichlorofluorescein, DCF) by cellular fROS, although DHR123 is converted to the fluorescent Rh123 by the oxidation [38, 40]. The DRGs were incubated in the presence of 4 μM DCFH-DA and DHR123 [37].

MitoTracker Red fluorescent stain is a cell permeable probe, and it labels mitochondrion with mildly thiol-reactive chloromethyl moiety. The Mito-fROS generation in the mitochondria imaged under the LSM800 microscope by using 150-nM MitoTracker Red CM-H2Xros fluorescent stain (Cell Signaling Technologies, Danvers, Massachusetts, USA), following the manufacturer's instructions [37].

For the assay of intracellular free Zn^{2+} ($[Zn^{2+}]_i$) concentration, the DRGs in the dishes with bottom glass were incubated with 1 μM Zn^{2+} labeling fluorescent dye (RhodZin3-AM, #F24195, Thermo Fisher Sci., Istanbul, Turkey). After washing the cells with extracellular buffer, the green images of RhodZin3-AM in the DRGs were captured in the LSM800 by using ZEN program of LSM800 [40].

ThiolTracker Violet (# T10095, Thermo Fisher Sci.) is an intracellular thiol probe for the GSH detection. Since GSH represents the majority of intracellular free thiols in the DRGs, ThiolTracker Violet (1 μl) was used in estimating the intracellular level of GSH, following the manufacturer's instruction. The green images of ThiolTracker Violet in the DRGs were captured in the LSM800 by using ZEN program of LSM800 [41].

The DRGs (1×10^6 cells/ml medium mixture) were incubated with the stains of Fluo-3AM, Hoechst 33342, PI, JC-1, DCFH-DA, DHR123, RhodZin3-AM, and ThiolTracker Violet for 60 min at 37 °C with 5% CO_2 in dark conditions [37, 40]. Then, the stains were removed from the media by washing (1xPBs). Lastly, the extracellular buffer with Ca^{2+} (400 μl) was added to the dishes of washed cells. The fluorescence intensities of Fluo-3AM, JC-1, DCF, Rh123, MitoTracker Red CM-H2Xros, and ThiolTracker Violet stains in the LSM800 microscope were expressed as arbitrary unit (a.u), although the rate of cell death was indicated as percentage changes.

In some analyses, the neurons of DRGs were treated by the antagonist of AMG (10 μM) to the inhibit Ca^{2+} entry before stimulation of TRPV1 (CAP and 10 μM).

The Assays of Apoptosis, Caspase 3 (CASP-3), Caspase -9 (CASP-9), Cell Viability, MMP, and Int-fROS in the Microplate Reader

A commercial programmed cell death (apoptosis) kit is Cell-APOPercentage (Biocolor Ltd. County Antrim, Northern Ireland) which allows the user to monitor the induction of apoptosis in the DRG and HIPPO. The commercial kit was used in the 96-black well plate of Infinite 200 PRO plate reader (Tecan Group Ltd., Männedorf, Switzerland) for the detection of apoptosis as described in previous studies [9, 13].

For the detection of CASP-3, we used a fluorogenic substrate (AC-DEVD-AMC). For the assay of active CASP-9, we used another fluorogenic substrate (AC-DEVD-AMC). The substrates were purchased from Bachem Inc. (Bubendorf, Switzerland), and they were analyzed in the 200 PRO microplate reader (Infinite 200 PRO). The excitation and emission detection wavelengths of AC-DEVD-AMC and ACDEVD-AMC were kept at 360 and 460 nm.

The MTT (0.5 mg/ml) was dissolved in the cell culture medium. In the cell viability analyses of DRG and HIPPO, the 100 µl MTT was added into each well of 96-well black plates, and it was incubated for 4 h at 37 °C. After washing the DMEM medium, 150 µl dimethyl sulfoxide was added to each well. The absorbance of the formazans was analyzed at 490 nm in the 200 PRO microplate reader.

The results of the apoptosis, CASP-3, CASP-9, and cell viability were presented as % of control.

In addition to the LSM800 analyses, we repeated the analyses of MMP (JC-1) and Int-fROS (DCFH-DA) in the DRG and HIPPO by using the 200 PRO microplate reader. The excitation emission details of the JC-1 and DCFH-DA were indicated in the previous studies [9, 13]. The results of the MMP and Int-fROS were also presented as % of control.

Western Blotting

The samples of proteins from the DRGs were separated on SDS-PAGE gels, and the samples of protein were transferred to the nitrocellulose membrane (Cat #1,620,112, Bio-Rad, Istanbul, Turkey). The membranes were incubated overnight at 4 °C with primary antibodies of TRPV1 (Cat #: ab6166), CASP-3 (Cat #: ab184787) (1: 200; Abcam), CASP-9 (Cat #: ab184786) (1: 200), and β-actin (Cat #: ab8226) (1: 200; Abcam, Istanbul, Turkey). The bands of the antibodies were imaged using the System of Gel Imagination (G:Box, Syngene, UK). After measuring the signal densities of antibodies using the program of ImageJ software, the data were shown as the relative density of control.

The Analyses of Lipid Peroxidation (MDA), Reduced Glutathione (R-GSH), Glutathione Peroxidase (GSHPx), and Antioxidant Vitamin Analyses in the Brain, Liver, Plasma, and Erythrocytes

For the preparation of the brain cortex and liver homogenates, the ultrasonic homogenizer (HD2200, Bandelin, Berlin, Germany) was used as described in the previous studies [36, 37]. The samples of plasma were obtained from the whole blood tube with anticoagulant (Disodium EDTA) by the centrifugation (500 g for 5 min). The remaining erythrocytes at the bottom of the tube were washed by the physiological saline, and the hemolysate of erythrocytes was prepared [36, 37]. The levels of MDA and R-GSH in the DRGs (10^6 in per ml) were analyzed at 532 and 412 nm by using the methods of Placer et al. [42] and Sedlak and Lindsay [43], respectively. The concentrations of MDA and R-GSH were indicated as µM per gram protein. The concentrations of total protein in the samples of brain, liver, and erythrocyte hemolysate were manually analyzed by using the Lowry's method [44].

For the assaying the GSHPx activity in the spectrophotometer, we used the method of Lawrence and Burk [45], and the activity of GSHPx was shown as international unit (IU) per gram protein.

The concentrations of vitamin A (retinol), β-carotene, and vitamin E (α-tocopherol) in the brain, liver, and plasma samples were spectrophotometrically analyzed at 340, 453, and 532 nm, respectively [46, 47]. The results of retinol, β-carotene, and α-tocopherol concentrations were shown as µmol/g tissue.

Statistical Analyses

For the detection of statistical significance, we used the one-way ANOVA of SPSS program. A post hoc test was employed when ANOVA indicated a statistically significant difference. The present data are represented as mean values ± standard deviation (SD). The presence of a $p \leq 0.05$ value was accepted as statistical significant after the Kruskal–Wallis analysis.

Results

The Treatment of NP Attenuated STZ-Mediated Levels of Mechanical Hyperalgesia, Heat Hyperalgesia, Body Weight Gain, and Blood Glucose Levels in the Rats

For assessment of mechanical and thermal pain sensitivity in rodents, Von Frey and hot plate tests have been used in several studies [2, 3, 13, 37]. Hence, we used both tests in the current study for peripheral neuropathy assessment of thermal and mechanical peripheral pain. DM induces the decrease of body weight, although it induces the increase of blood glucose levels. However, the effects of NP on the blood glucose and body weight gain have not been clarified yet. For 42 days after the injection of STZ, we gradually observed a significant increase in the mechanical, heat withdrawal threshold, and blood glucose (Fig. 1d) as demonstrated by von Frey (Fig. 1a), hot plate (Fig. 1b), and glucometer assessments, respectively. However, body weight gains in the groups of STZ were gradually decreased during the 42 days after the STZ injection (Fig. 1c) ($p \leq 0.05$). On the other word, the treatment of STZ caused to the increase of mechanical hyperalgesia, heat hyperalgesia, and blood

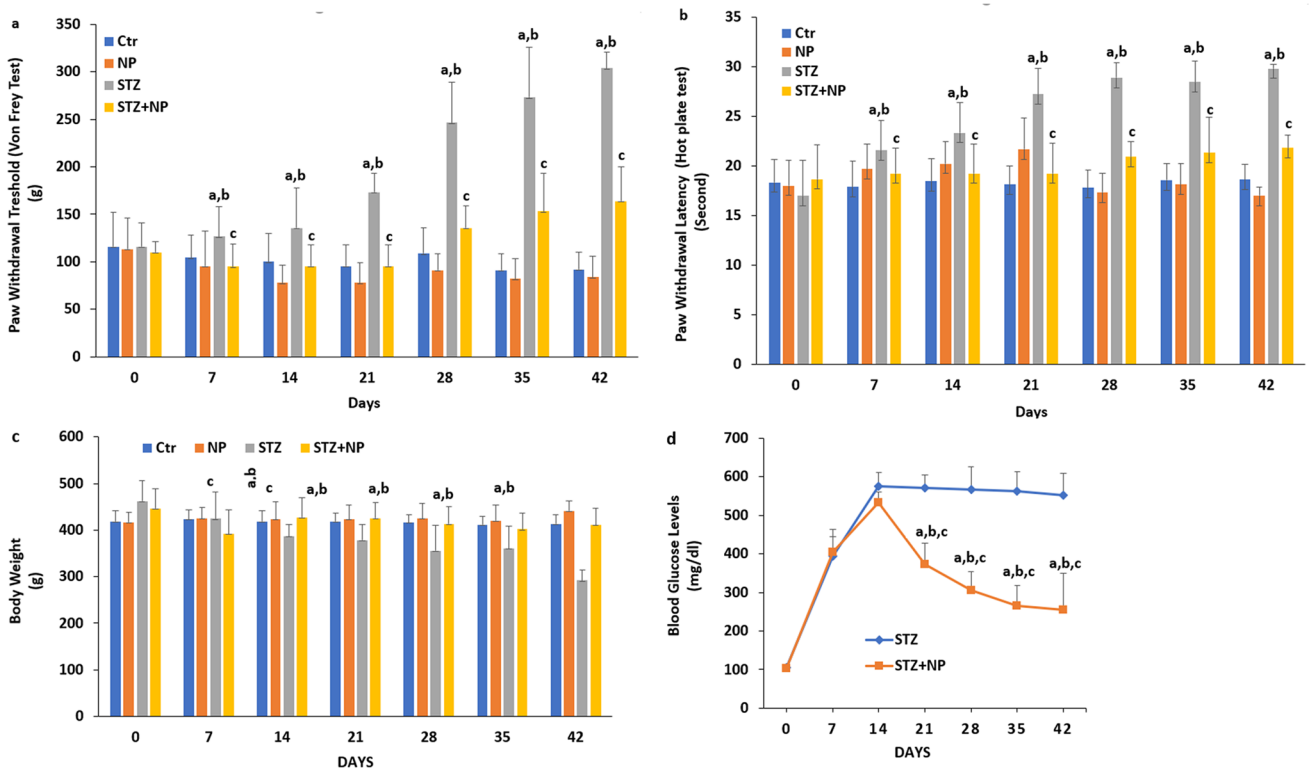

Fig. 1 The treatment of Noopept (NP) modulated diabetes (STZ)-induced paw withdraw threshold [the Von Frey Test (**a**) and Hot Plate Test (**b**)], body weight gain (**c**), and blood glucose changes (**d**) in the rats. ($n=9$ and mean ± STD). ($^{a}p \leq 0.05$ *vs* 0 day. $^{b}p \leq 0.05$ *vs* control (Ctr) and NP groups. $^{c}p \leq 0.05$ *vs* STZ group

glucose, although it induced the decrease of body weight gain on days 7, 14, 21, 28, 35, and 42 as compared with the control and NP groups as well as 0 day ($p \leq 0.05$). After the NP injections, the potent antihyperalgesic, blood glucose increase, and body weight modulator actions of NP treatment were observed in the rats ($p \leq 0.05$).

STZ-Induced Increase of Intracellular free Ca^{2+} ($[Ca^{2+}]i$) Concentration Was Decreased via Modulation of TRPV1 in the DRGs and HIPPO by the Treatment of NP

For investigating the interactions between NP and the TRPV1-mediated $[Ca^{2+}]_i$ concentration in diabetes, we performed three analyses, namely, Fura-2, Fluo-3, and patch-clamp. In the Fura-2 florescent and Fluo-3 imaging analyses, the TRPV1 channel in the DRGs and HIPPO in the NP- and STZ-treated group were gated by CAP (10 μM). Within 0.36 ± 0.13 min, stimulations with CAP induced an increase in the $[Ca^{2+}]_i$ concentration in the DRGs (Figs. 2a, b, and c) and HIPPO (Figs. 2d, e, and f) of STZ and NP treated rats, because of the activation of Ca^{2+}-permeable TRPV1 ($p \leq 0.05$). The concentration of $[Ca^{2+}]_i$ in the neurons of DRG and HIPPO was higher in the STZ group than in the control and NP groups (Figs. 2a, b, d, and e), although they were effectively decreased in the neurons by the groups of STZ + AMG ($p \leq 0.05$).

Image results of Fluo-3 in the groups of control, NP, STZ, STZ + NP, and STZ + PJ34 are shown in Fig. 3a. In addition, the changes of Fluo-3 florescence intensity in the groups of STZ and STZ + NP within 18 min are shown in the Fig. 3b and 3c, respectively. Without CAP stimulation, the Fluo-3 florescence intensity in the group of STZ was higher than in the groups of control and NP ($p \leq 0.05$) (Figs. 3d), although its concentration was further increased in the STZ group by the CAP stimulation. The increase was not observed in the groups of STZ + NP and STZ + PJ34 after the CAP stimulation. However, the Fluo-3 florescence intensity was reduced in the groups of STZ + NP and STZ + PJ34 by the treatments of TRPV1 antagonist (AMG) and PARP1 inhibitor (PJ34), and its concentration was lower in the groups of STZ + NP and STZ + PJ34 than in the group of STZ only (Figs. 3d and e).

The results of Fura-2 and Fluo-3 clearly indicated that the STZ-mediated increase of $[Ca^{2+}]_i$ concentration in DRGs and HIPPO was decreased via regulation of TRPV1 by the treatment of NP.

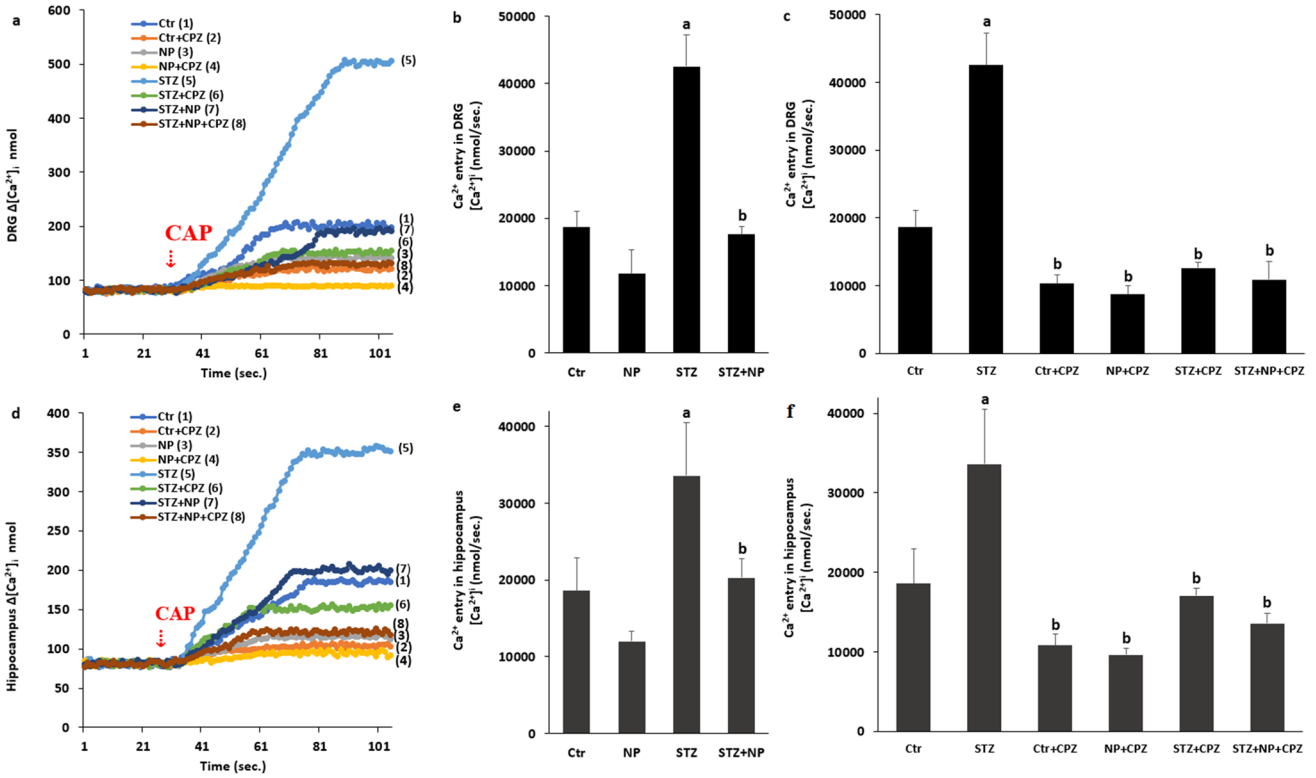

Fig. 2 The treatment of noopept (NP) attenuated diabetes (STZ)-induced increase of $[Ca^{2+}]_i$ concentrations through a block of the TRPV1 in the DRG and HIPPO of rats. ($n=9$ and mean ± STD). The animals received intraperitoneal NP for 6 weeks after a single dose of STZ injection. Then, these dissected neurons from DRG and HIPPO of control, NP, STZ, and STZ + NP groups were further in vitro treated with CAP (10 μM) and CPZ (0.1 mM) before loading Fura-2 for 100 s. The STZ-induced increase of $[Ca^{2+}]_i$ concentration was decreased in the DRG (**a, b,** and **c**) and HIPPO (**d, e,** and **f**) by NP and CPZ treatments. ([a] $p \leq 0.05$ *vs* control (Ctr) and NP groups. [c] $p \leq 0.05$ *vs* STZ group)

The STZ-Induced Increase of TRPV1 Current Density in the DRGs Was Diminished by the Treatment of NP

The current density results of path-clamp analyses with whole cell (W.C.) configuration are shown in Fig. 4. Without CAP stimulation, there was no current of TRPV1 in the cells (Fig. 4a). However, the TRPV1 was activated by the addition of CAP (10 μM) into the patch chamber solution [Figs. 4b and b (I-V)]. The mean activation times of TRPV1 in the Ctr + CAP and STZ + CAP groups were 3.89 ± 0.49 and 1.93.063 min, respectively. The activation time of TRPV1 is markedly shorter in the STZ + CAP group than in the Ctr + CAP group ($p \leq 0.05$). The densities of TRPV1 currents were higher in the Ctr + CAP group (118.08 pA/pF) than in the Ctr group (6.21 pA/pF) (Fig. 4f) ($p \leq 0.05$). The current densities of TRPV1 were further increased in the STZ + CAP group (183.72 pA/pF) [Figs. 4c (I-V)] as compared with Ctr + CAP group ($p \leq 0.05$). The densities of TRPV1 current were lower in the Ctr + CAP + AMG (30.20 pA/pF) and STZ + CAP + AMG (40.17 pA/pF) groups than in the Ctr + CAP and STZ + CAP groups ($p \leq 0.05$). By the treatment of NP with STZ (Fig. 3d) without STZ (Fig. 3e), there was no increase of TRPV1 currents via CAP stimulation. The mean densities of TRPV1 currents were significantly ($p \leq 0.05$) lower in the STZ + NP + CAP (6.38 pA/pF) and NP + CAP (5.08 pA/pF) groups as compared with the groups of Ctr + CAP (118.08 pA/pF) and STZ + CAP (183.72 pA/pF) ($p \leq 0.05$). The present patch-clamp TRPV1 current results further confirmed the modulator action of NP on the STZ-mediated excessive Ca^{2+} influx via TRPV1 activation in the DRGs.

The Apoptotic and Neuronal Death Actions of STZ Were Diminished in the DRGs and HIPPO by the Inhibitions of TRPV1 and Caspases

More recent data have reported a function of Ca^{2+} also in the regulations of DRGs and HIPPO death [2, 3]. The results of recent reports indicated that the programmed cell death (apoptosis) is induced via the stimulation of CASP-3 and CASP-9 in the DRGs and HIPPO of diabetic rats by the increase of $[Ca^{2+}]_i$ concentration [13, 15, 16]. Hence, the Ca^{2+} influx through Ca^{2+} channels, including the TRPV1 channel, has been proposed to be apoptotic

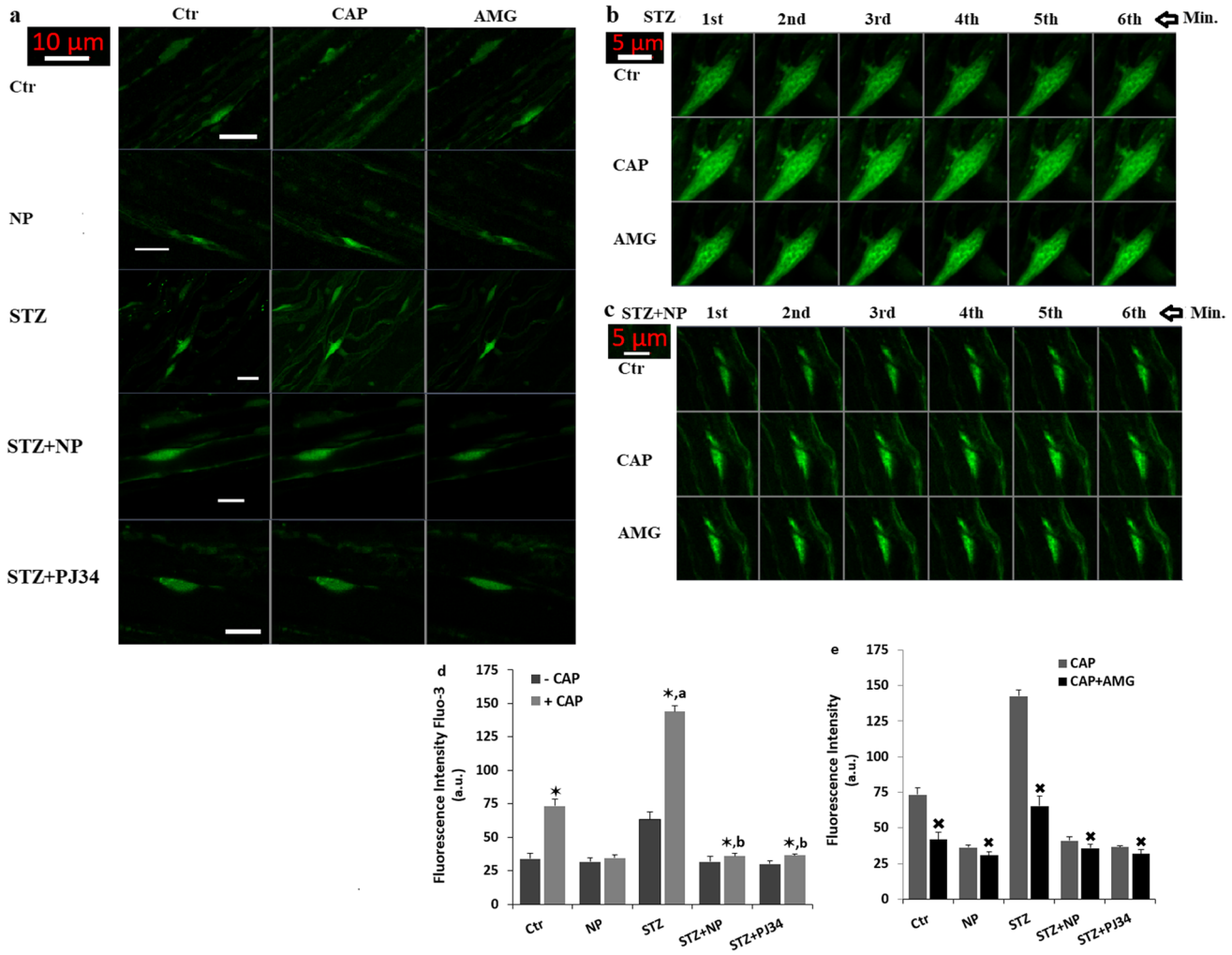

Fig. 3 The treatment of noopept (NP) modulated diabetes (STZ)-induced the increase of $[Ca^{2+}]_i$ in the whole DRG. (Mean ± SD). The DRGs were stained with Fluo-3 (1 µM for 1 h). After washing the DRGs with 1xPBS, they were stimulated with CAP (10 µM for 5 min) and then they were inhibited by AMG (10 µM for 5 min) in the LSM 800 with 40×oil objective. The representative images of the Fluo-3 in the five groups [control (Ctr), NP, STZ, STZ + NP, and STZ + PJ34] were shown in the Fig. 3a. The changes of fluorescence intensity within 18 min in the groups of STZ and STZ + NP are shown in the Figs. 3b and c, respectively. The changes of mean fluorescence intensities as arbitrary unit (a.u.) in the five groups after the CAP and AMG treatments are shown in the Figs. 3d. The modulator role of AMG treatment on the CAP-mediated increase of Fluo-3 fluorescence intensity in the DRGs is shown in the Fig. 3e by the columns. The scale bar in the images was kept as 5 µm. One represented image of each figure was selected from 25–30 cells of 9 independent experiments for each condition. ($^a p \leq 0.05$ *vs* the groups of Ctr and NP. $^b p \leq 0.05$ *vs* the groups of STZ. $p \leq 0.05$ *vs* without CAP stimulation (- CAP group). $p \leq 0.05$ *vs* CAP stimulation (+ CAP group)

and caspase stimulator properties in the neurons of diabetic animals [13, 15, 16]. The protective action of NP against the activation of TRPV1 in the diabetic DRGs and HIPPO has not been reported yet. For clarifying the modulator action of NP on the STZ-induced programmed cell death, we investigated the levels of cell death (PI/Hoechst rate), apoptosis, cell viability (MTT), CASP-3, and CASP-9 in the DRGs and HIPPO. The BF (Fig. 5a), red/blue PI/Hoechst (Fig. 5b), and 2.5 images (Fig. 5c) of PI/Hoechst indicated that STZ induced the increase of DRG death in the STZ group as compared with the control and NP groups ($p \leq 0.05$). However, the DRG death action of STZ was diminished in the STZ + NP and STZ + AMG groups by the treatments of NP and AMG ($p \leq 0.05$). Similar changes were observed on levels of cell viability, apoptosis, CASP-3, and CASP-9 in the DRGs and HIPPO. The levels of apoptosis (Fig. 6a), CASP-3 (Fig. 6b), and CASP-9 (Fig. 6c) were increased

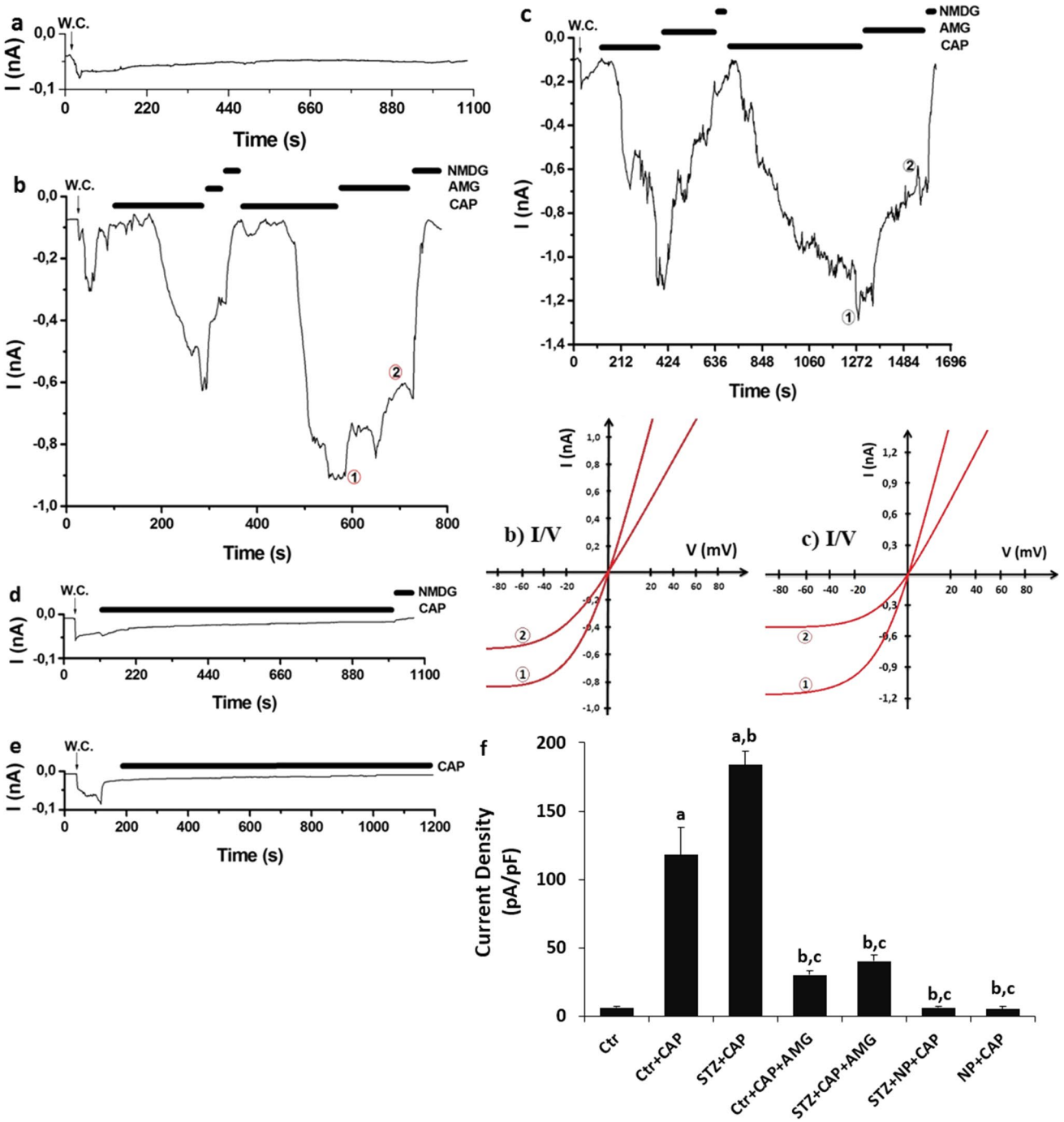

Fig. 4 The STZ-mediated-increase of TRPV1 current density in the DRGs was decreased by the treatment of NP. (n = 9 and mean ± SD). The TRPV1 in the DRGs was stimulated by the CAP (10 μM), although it was blocked by the treatment of AMG (10 μM). The whole cell patch-clamp configuration was abbreviated as W.C. **a** Control (Ctr) (without CAP). **b** Ctr + CAP group with the treatment of CAP and AMG. **c** STZ + CAP group with the treatment of CAP and AMG after the diabetes (STZ) induction. **d** STZ + NP + CAP group with the treatments of STZ, CAP, and AMG. **e**. NP + CAP group (without STZ treatment). **f** The mean densities of TRPV1 currents. **b) I/V** and **c) I/V**. Current (I)-voltage (V) relationship of the Figs. b and c, respectively. ($^{a}p \leq 0.05$ *vs* Ctr. $^{b}p \leq 0.05$ *vs* the group of Ctr + CAP. $^{c}p \leq 0.05$ *vs* the group of STZ + CAP)

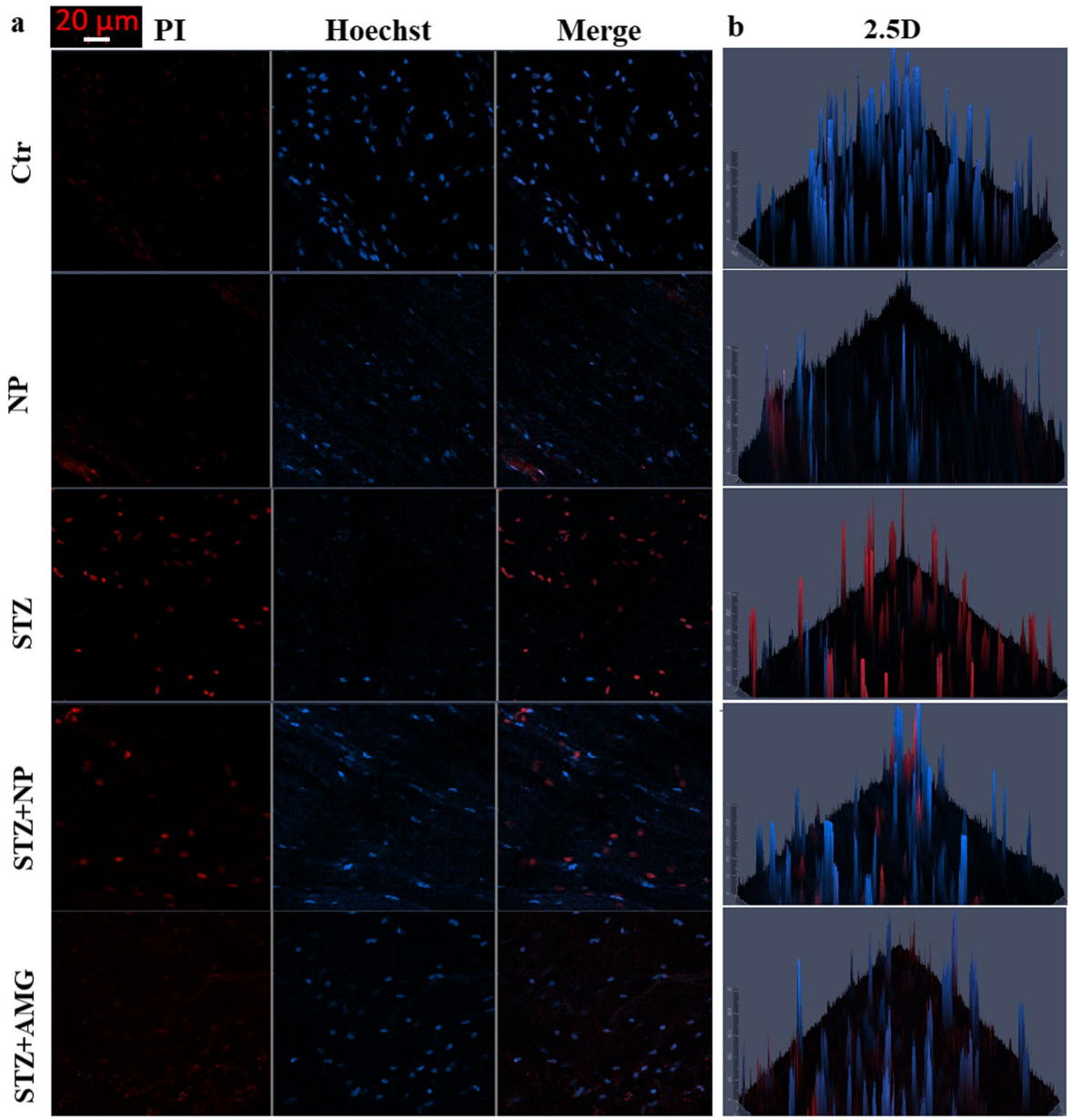
a
20 μm
PI
Hoechst
Merge
b
2.5D
Ctr
NP
STZ
STZ+NP
STZ+AMG
c
Cell Death (PI/Hoechst) Rate (%)
70
60
50
40
30
20
10
0
*
**
**
Ctr
NP
STZ
STZ+NP
STZ+AMG

◂**Fig. 5** The treatments of NP and AMG modulated STZ-mediated DRG death. (Mean ± SD and $n = 25–30$). **a** The images of bright field (BF, black-white). (Objective: 20×. Scala bar: 50 μm). **b** The images of red-PI (dead cells), blue-Hoechst (live cells), and their merge. **c** 2.5D images of PI and Hoechst. (Objective: 20×. Scala bar: 50 μm). **d** The mean percentage of PI and Hoechst-positive cells in the Ctr, NP, STZ, STZ + NP, and STZ + AMG groups. ($^{*}p \le 0.05$ *vs* the groups of control (Ctr) and NP. $^{**}p \le 0.05$ *vs* the group of STZ)

in the STZ group as compared with the groups of control and NP, although the level of cell viability (Fig. 6b) was decreased in the STZ group ($p \le 0.05$). However, the treatments of NP and TRPV1 antagonist (AMG) acted the modulator role on the STZ-induced increase of apoptosis, cell viability, and caspases in the DRGs and HIPPO of STZ group ($p \le 0.05$).

The Treatments of NP and TRPV1 Antagonist (AMG) Decreased STZ-Mediated Increase of Oxidative Stress and MMP in the DRGs and HIPPO

Another hallmark of the excessive Ca^{2+} influx is the loss of MMP via opening the mitochondrial permeability transition pore (mPTP) triggered in the DRGs and HIPPO [13, 48]. The increase of MMP via the TRPV1-mediateed increase of excessive Ca^{2+} influx results in the increase of Int-fROS and Mito-fROS in the DRGs

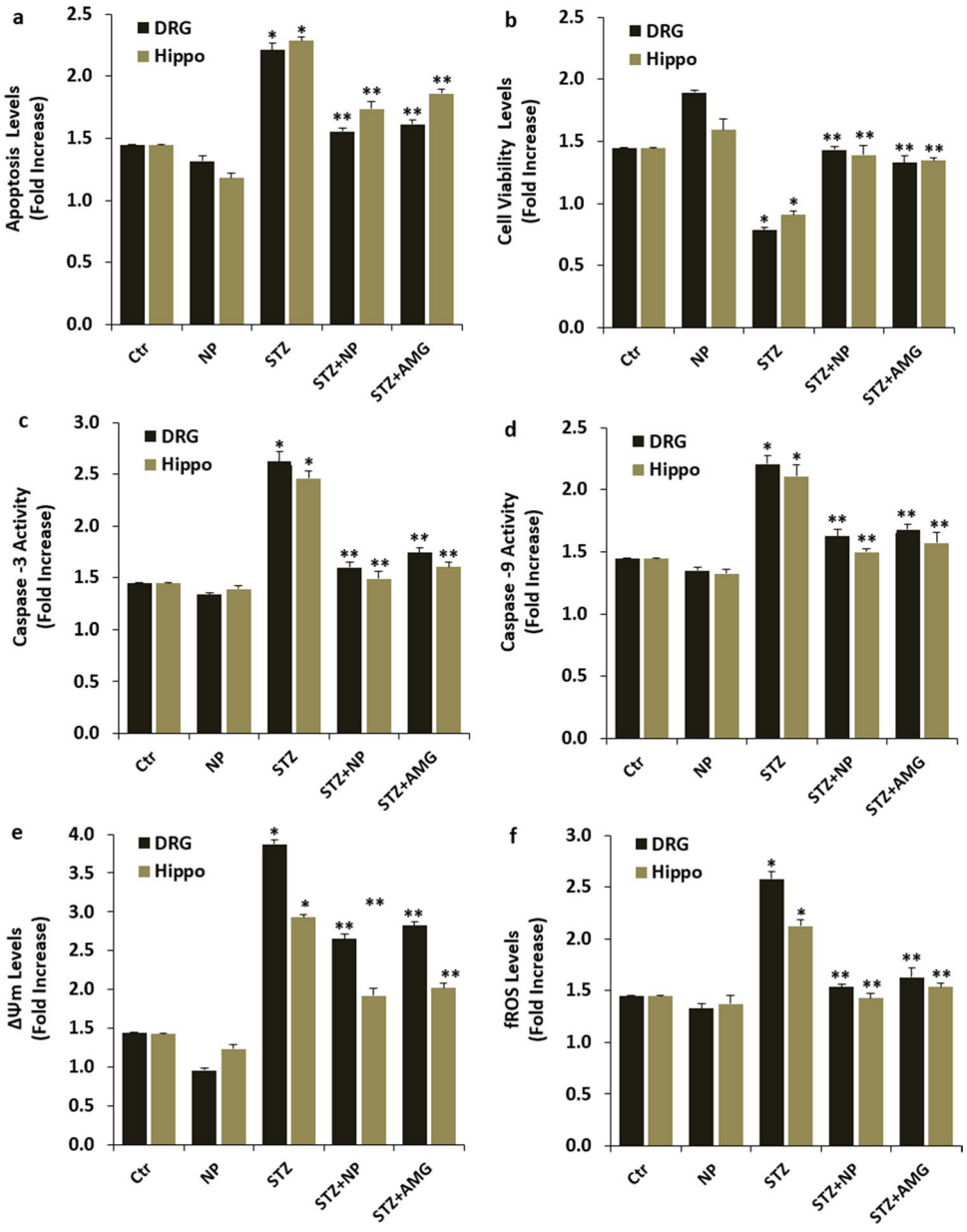

Fig. 6 The treatments of NP and AMG attenuated STZ-mediated the increase of apoptosis, cell viability, CASP-3, CASP-9, mitochondrial membrane potential (ΔΨm), and intracellular fROS (Int-fROS) generation in the DRGs and HIPPO of rats (Mean ± SD and $n = 9$). The black bars of **a**, **b**, **c, d, e,** and **f** are representing the changes of apoptosis, cell viability (MTT), CASP-3, CASP-9, ΔΨm, and Int-fROS in the DRGs and HIPPO of five groups, respectively. The six assays were performed in the five groups by using the microplate reader. ($^{*}p \le 0.05$ *vs* the groups of control (Ctr) and NP. $^{**}p \le 0.05$ *vs* the group of STZ)

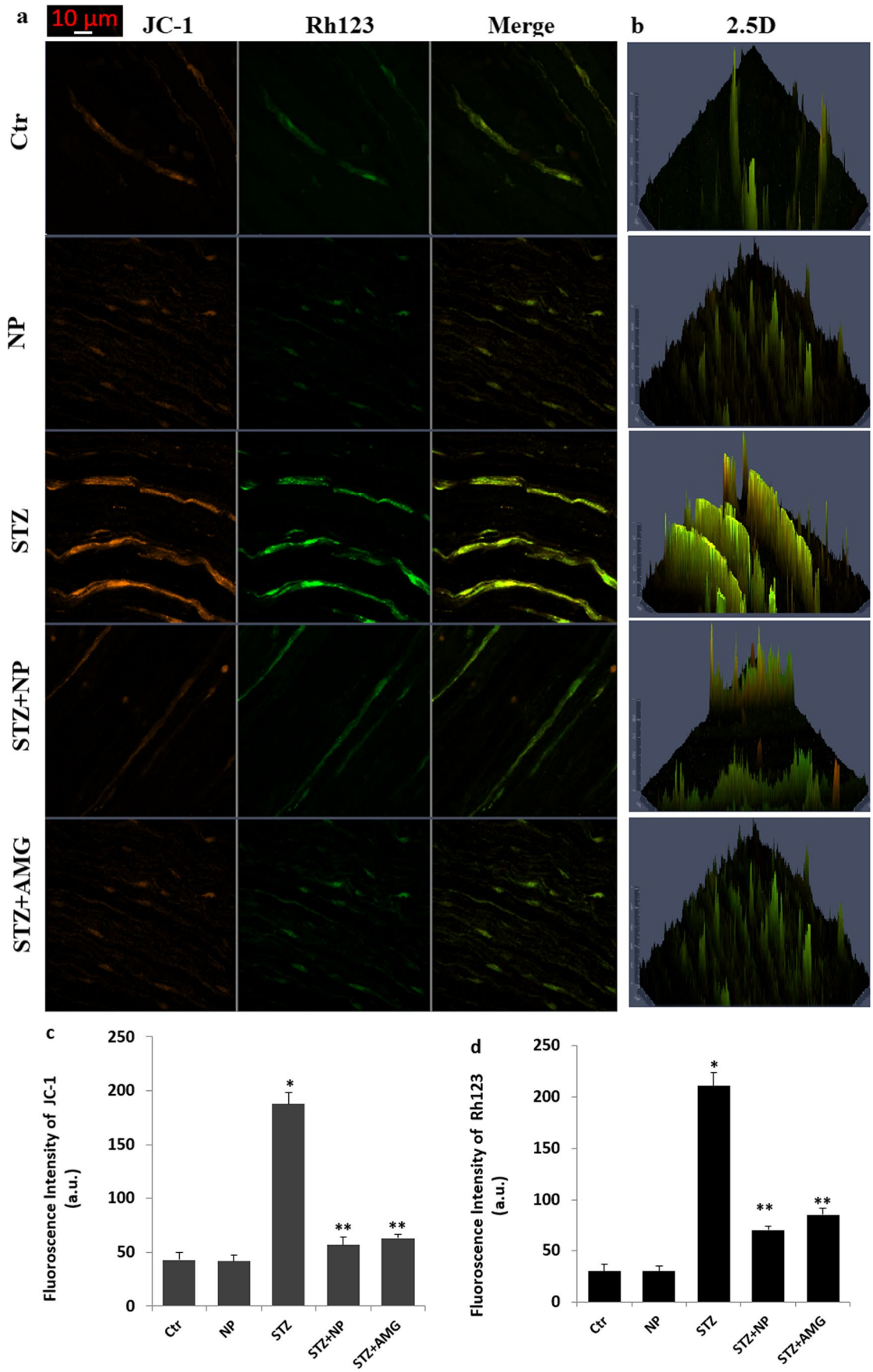
a
10 μm
JC-1
Rh123
Merge
b
2.5D
Ctr
NP
STZ
STZ+NP
STZ+AMG
c
Fluoroscence Intensity of JC-1 (a.u.)
250
200
150
100
50
0
*
**
**
Ctr
NP
STZ
STZ+NP
STZ+AMG
d
Fluoroscence Intensity of Rh123 (a.u.)
250
200
150
100
50
0
*
**
**
Ctr
NP
STZ
STZ+NP
STZ+AMG

◂**Fig. 7** The STZ-mediated increases of mitochondrial membrane depolarization (MMP, JC-1) and Int-fROS (Rh123) were diminished in the DRGs by the treatments of NP and AMG. (Mean ± SD and $n = 25–30$). The DRGs were stained with 2 μM JC-1 and DHR123 (**a** and **b**) for measurements of MMP and Rh123, respectively. The florescence intensities in the images of LSM800 microscope (20 × objective) were calculated by using the ZEN program. The data of JC-1 (**c**) and Rh123 (**d**) are presented as arbitrary units (a.u.) by columns. ($^{*}p \le 0.05$ *vs* the groups of control (Ctr) and NP. $^{**}p \le 0.05$ *vs* the group of STZ)

and HIPPO [15, 16]. After observing the increase of the $[Ca^{2+}]_i$ concentration in the DRGs and HIPPO of STZ group, we suspected the increase of MMP, Int-fROS, and Mito-fROS in the DRGs and HIPPO of STZ group. Hence, we evaluated the changes via probes of MMP (JC-1), Int-fROS (DCF and Rh123), and Mito-ROS in the microplate reader and LSM microscope. The images and fluorescence intensity of MMP levels (Figs. 6e and 7a, b, and c), Rh123 (Figs. 7a, b, and d), DCF (Figs. 6f, and 8a, b, and d), and Mito-fROS (Figs. 8a, b, and c) indicated that the levels of MMP, Int-fROS, and Mito-fROS in DRGs and HIPPO of STZ group were increased in the STZ group as compared with the control and NP groups ($p \le 0.05$). However, their levels were markedly decreased in the STZ + AMG group by the treatment of AMG.

The Treatments of NP and TRPV1 Antagonist (AMG) Modulated STZ-Mediated the Changes of $[Zn^{2+}]_i$ and GSH in the DRGs

The level of $[Zn^{2+}]_i$ (Figs. 9a and c) was increased in the STZ group as compared with the groups of control and NP, although the level of and GSH (Fig. 9b and d) was decreased in the STZ group ($p \le 0.05$). However, the treatments of NP and TRPV1 antagonist (AMG) acted the modulator role on the STZ-induced changes of $[Zn^{2+}]_i$ and GSH in the DRG STZ group ($p \le 0.05$).

STZ-Mediated the Decrease of MDA, R-GSH, GSHPx, and Fat-Soluble Antioxidant Vitamin Concentrations Were Attenuated by the Treatment of NP

Numerous literature data indicated the decrease of MDA, R-GSH, GSHPx, and fat-soluble antioxidant vitamin concentrations in the brain, liver, kidney, erythrocyte, and plasma of human and experimental animals, although the modulator role of NP on the concentrations in the tissues has not been clarified yet [8, 13, 36]. After observing the modulator role of NP on the Int-fROS and Mito-fROS in the DRG and HIPPO of diabetic rats, we suspected the modulator role of NP on the changes of MDA, R-GSH, GSHPx, and fat-soluble antioxidant vitamin concentrations in the brain, liver, kidney, erythrocyte, and plasma of rats with diabetes. The concentrations of MDA, R-GSH, GSHPx, vitamin E, and β-carotene in the brain, erythrocytes, kidney, liver, and plasma were higher in the group of STZ than in the groups of control and NP ($p \le 0.05$) (Table 1). However, the increase of MDA, R-GSH, GSHPx, vitamin E, and β-carotene in the brain, erythrocytes, kidney, liver, and plasma was decreased in the STZ + NP group by the treatment of NP ($p \le 0.05$). The concentration of vitamin A was not changed in the four groups ($p \ge 0.05$).

STZ-Mediated Increase of TRPV1, CASP-3, and CASP-9 Expression Levels in the DRGs Were Attenuated by the Treatment of NP

In addition to the plate reader analyses, we further investigated the levels of CASP-3 and CASP-9 by the Western blot analyses. The increases of DNP and $[Ca^{2+}]_i$ concentration are induced in the DRGs by the increase of TRPV1. The STZ-induced increase of TRPV1 expression was reported in the DRGs [49], although there is no report of NP treatment on the TRPV1 expression level in the DRGs. In addition to the expression levels CASP-3 and CASP-9, we investigated the protective role of NP treatment on the TRPV1 expression level in the DRGs. The expression levels of TRPV1 (Figs. 10a and b), CASP-3 (Figs. 10a and c), and CASP-9 (Figs. 10a and d) in the DRGs were higher in the group of STZ than in the groups of control and NP, although their expression levels were decreased in the STZ + NP group by the treatment of NP ($p \le 0.05$).

Discussion

A common complication of DM is DNP. Patients with DM are extensively suffering from the DNP. The excessive Ca^{2+} influx and fROS generation via the activation of TRPV1 are considered to be the most important pathogenetic factors in the etiology of DNP [20, 49, 50]. Accumulating data suggest that NP is an effective antioxidant because of its excellent action agents to the neuronal oxidative cytotoxicity [26, 32, 33]. Hence, the antioxidant NP may modulate the DPN and HIPPO neurotoxicity via inhibition of TRPV1, apoptosis, and fROS in the DRGs and HIPPO of STZ-induced rats. In the current study, we observed the increase of DNP, Mito-fROS, apoptosis, oxidative stress, caspase activations, TRPV1 expression levels in the DRGs and HIPPO of STZ-treated rats, although cell viability, GSHPx, R-GSH, vitamin E, and

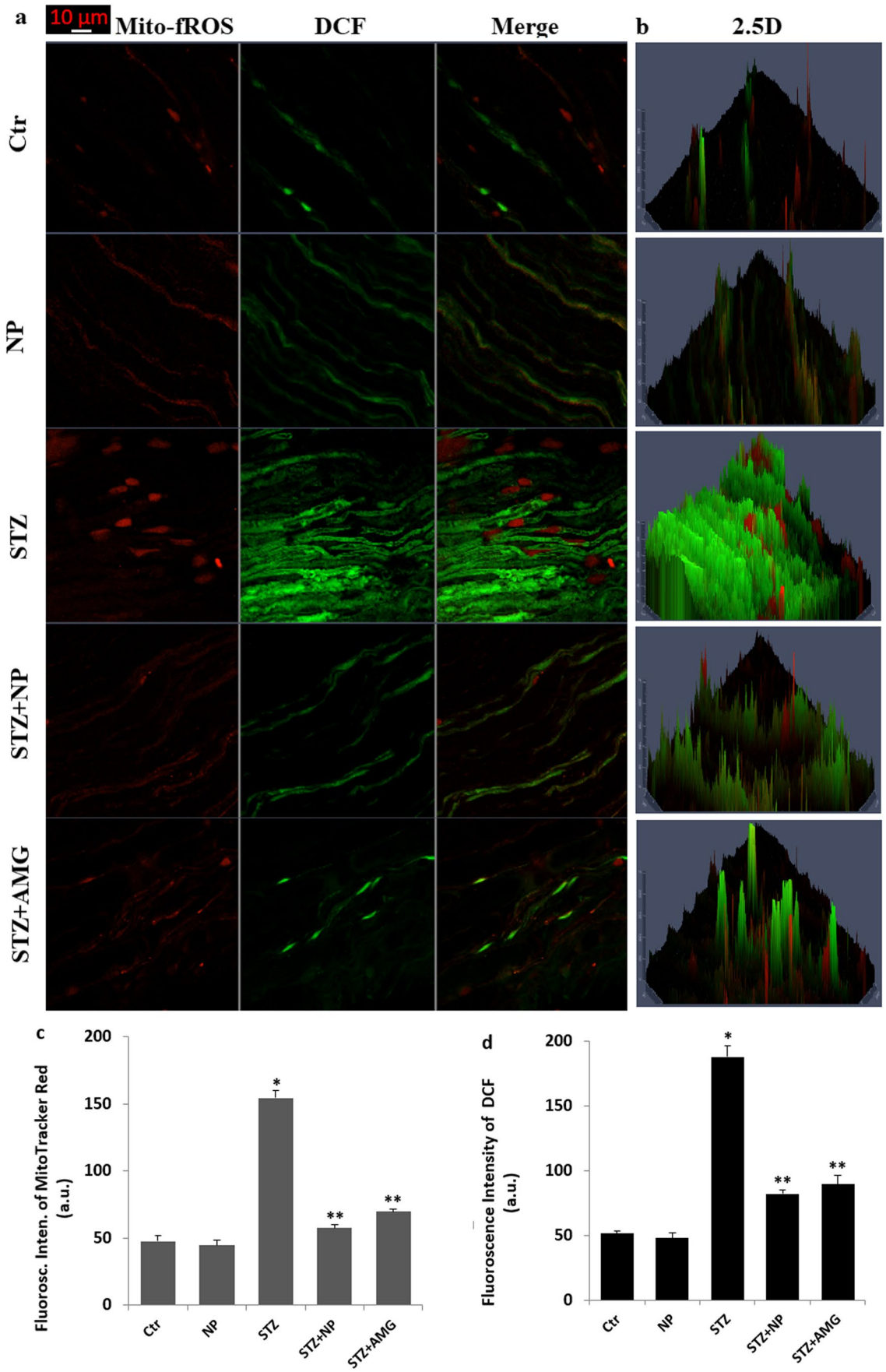
a
10 μm
Mito-fROS
DCF
Merge
b
2.5D
Ctr
NP
STZ
STZ+NP
STZ+AMG
c
Fluorosc. Inten. of MitoTracker Red (a.u.)
200
150
100
50
0
*
**
**
Ctr
NP
STZ
STZ+NP
STZ+AMG
d
Fluoroscence Intensity of DCF (a.u.)
200
150
100
50
0
*
**
**
Ctr
NP
STZ
STZ+NP
STZ+AMG

◂**Fig. 8** The STZ-mediated increases of mitochondrial fROS generation (Mito-fROS) and Int-fROS (DCF) were reduced in the DRGs by the treatments of NP and AMG. (Mean ± SD and n = 25–30). The DRGs were stained with 150 nM MitoTracker Red CM-H2Xros and 5 μM DCFH-DA (**a** and **b**) for measurements of Mito-fROS and DCF, respectively. The florescence intensities in the images of LSM800 microscope (20 × objective) were calculated by using the ZEN program. The data of Mito-fROS (**c**) and DCF (**d**) are presented as arbitrary units (a.u.) by columns. ($^{*}p \leq 0.05$ *vs* the groups of control (Ctr) and NP. $^{**}p \leq 0.05$ *vs* the group of STZ)

β-carotene concentrations were decreased. The changes were modulated in the DRGs and HIPPO by the NP and TRPV1 agonist (AMG). These data suggest that the treatment of NP modulated DNP, apoptosis, and fROS via the inhibition of STZ-activated TRPV1 channel in the DRGs and HIPPO.

A member of TRP superfamily is the TRPV1 channel. The agonist role of CAP and antagonist role of AMG on the activation TRPV1 in the DRGs and HIPPO were recently reported [20, 21]. In the current study, we observed similar results. The current densities and fluorescence intensities of TRPV1 were inhibited in the DRGs and HIPPO after the CAP stimulation. In addition to the CAP stimulation, TRPV1 is activated in the DRGs and HIPPO by several stimuli, including fROS [13, 18, 51]. Hence, the STZ-mediated TRPV1 activation was inhibited in the DRGs and HIPPO by the antioxidants such as selenium and alpha-lipoic acid [13, 50]. In the current study, STZ-mediated fROS and TRPV1 activation were diminished by the treatment of NP. Similarly, the antioxidant action of NP was reported in the HIPPO of rats [26, 32, 33]. The modulator role of NP via inhibition of voltage gated Ca^{2+} channels on the Ca^{2+} influx in the HIPPO was also reported [31].

The increased serum Ca^{2+} level is shown to be correlated with fasting blood glucose levels and insulin resistance. Furthermore, studies have shown intracellular Ca^{2+} level to be effective in glucose homeostasis and DNP [2, 15, 16]. Hyperglycemia-mediated increase of the $[Ca^{2+}]_i$ concentration causes oxidative stress, also rises of regional Ca^{2+} concentration in the damage area or spinal canal has been reported to cause neuropathic pain [3, 5–7]. Hence, a main source of pain, including DNP is the excessive Ca^{2+} influx. However, the DNP intensity was decreased in rats by the decrease of $[Ca^{2+}]_i$ concentration via the inhibition of cation channels, including TRPV1 channels [7, 14]. The STZ-mediated TRPV1 activation induced DNP in the rats, although its inhibition via antioxidant decreased the STZ-induced DNP in the animals [13, 50]. Similarly, the increase of $[Ca^{2+}]_i$ concentration via the inhibition of TRPV1in the current data was decreased in the DRGs and HIPPO by the treatment of NP. In turn, the increase of mechanical and thermal DNP was reduced by the treatment of NP. Hence, the decrease of STZ-mediated DNP was confirmed by the current results of $[Ca^{2+}]_i$ concentration.

The thiol redox system has an essential role on the scavenge of fROS in the cells of mammalian. Members of the thiol redox system are synthetized from cysteine [52]. The recent data indicated that some TRP channels, including the TRPV1 are activated via the oxidation of cysteine groups in the channel proteins by the excessive generation of fROS [53, 54]. The antioxidants such as GSH, R-GSH, GSHPx, and α-lipoic acid are members of the thiol-cysteine redox system [13, 50, 52]. Hence, the treatment of antioxidants or supporting the antioxidants in body decreases the generations of Int-fROS and Mito-fROS [13, 50] (Fig. 11). In the current study, the STZ-mediated decrease of the GSH, R-GSH, and GSHPx levels were increased in the DRGs and HIPPO by the treatment of NP, although the levels of lipid peroxidation, Int-fROS, and Mito-fROS were decreased by the treatment. Synergically, the TRPV1 activity was also decreased by the treatment of NP. It seems that the NP treatment inhibited the STZ-mediated TRPV1 activation via supporting the GSH redox system.

The accumulation of $[Ca^{2+}]_i$ concentration via the activation of TRPV1 induces the increase of MMP in the mitochondria [7, 55]. In turn, it induces apoptosis and cell death via the activation of CASP-3 and CASP-9 in the DRGs and HIPPO [13, 50]. As a cognitive enhancer, NP has proven neuroprotective properties on cell viability, ROS level, and mitochondrial function in neurons [26, 32, 33]. The results of Ostravskaya et al. [33–35] indicated that the treatment of NP increased the neurotrophic factors in neurons, and NP acted antiapoptotic effect with the prevention of DM-induced atypical DNA comet formation. Although there are studies on apoptosis in normal HIPPO, there is no report of NP on the levels of cell death, apoptosis, CASP-3, and CASP-9 in the DRGs and diabetic HIPPO till today [21, 25]. In the analyses of microplate reader and Western blot, we have determined the protective role of NP on the STZ-mediated increase of cell death in the DRGs and HIPPO. The determined neuroprotective effect of NP is not only important for homeostatic and cognitive brain impairments but also for peripheric neural activity in the chronic diabetic process.

The oxygen metabolism rate of the brain and erythrocytes are high, although they have low antioxidant levels. In addition, the STZ-mediated oxidative stress has a main injury action on the liver and kidney in rats [36]. The fat-soluble antioxidant vitamins, vitamin E and β-carotene, are scavengers of several radicals such as hydroxyl radical and singlet oxygen radical [56]. The decreases of vitamin E and β-carotene concentrations

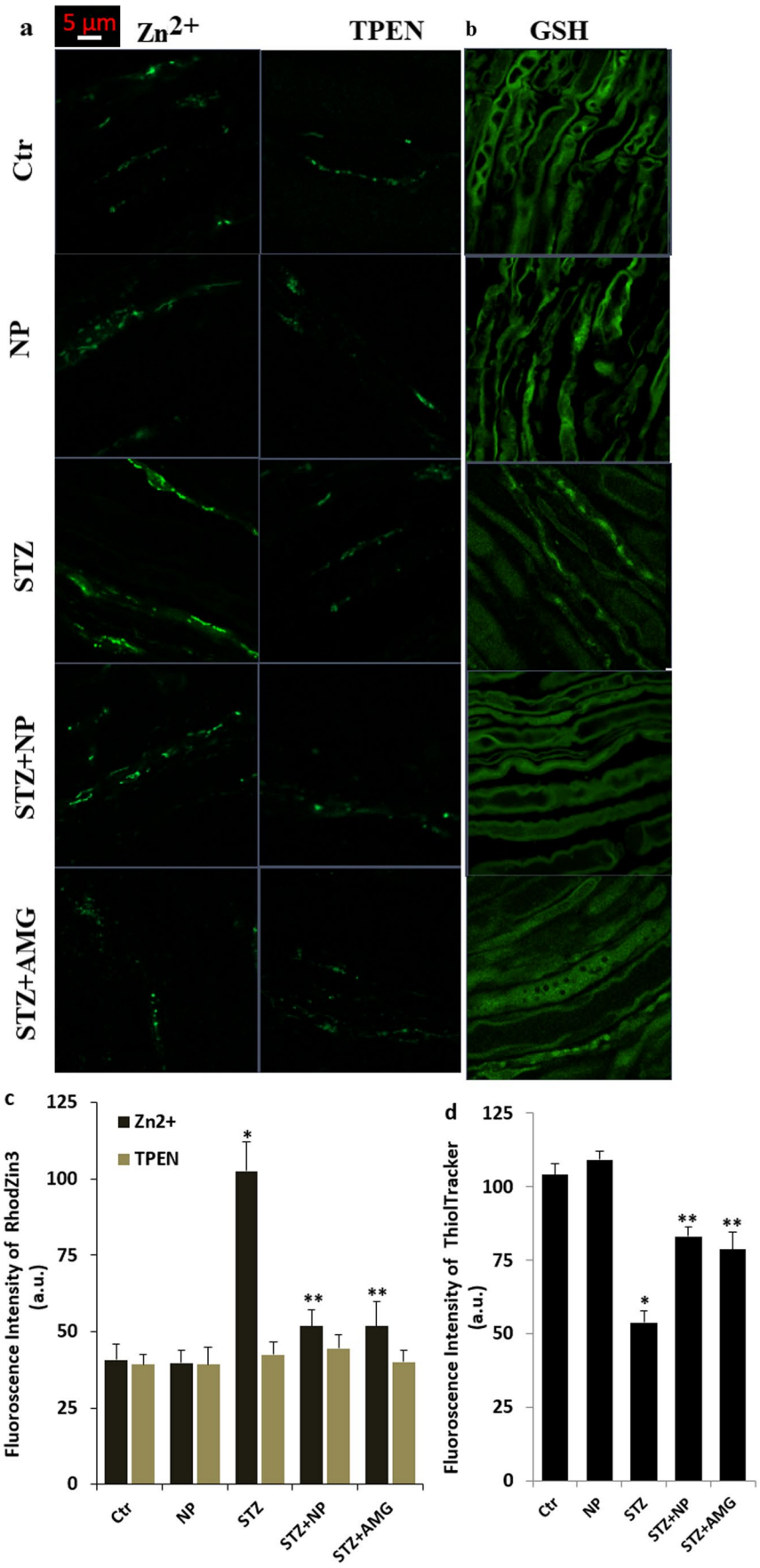

Fig. 9 STZ-mediated the increase of cytosolic free Zn^{2+} ($[Zn^{2+}]_i$) concentration was decreased in the DRGs by the treatments of NP and AMG, although GSH concentration was increased by the treatments. (Mean ± SD and n = 25). The DRGs were stained with 1 mM RhodZin3-AM and Thiol-Tracker™ Violet for assaying the concentration of $[Zn^{2+}]_i$ and GSH, respectively. The DRGs were also incubated by the blocker of $[Zn^{2+}]_i$ (1 μM, TPEN). The RhodZin3-AM-TPEN and GSH images were indicated in Figs. 9a and b, respectively. Fluorescence intensities as a.u. of the RhodZin3-AM (a), TPEN (a), and GSH (**c**) are presented by columns. The samples in the groups of the Ctr, NP, STZ, STZ + NP, and STZ + AMG were analyzed by the LSM800 (Objective: 20×. Scala bar: 5 μm). ($^{*}p \leq 0.05$ *vs* the groups of control (Ctr) and NP. $^{**}p \leq 0.05$ *vs* the group of STZ)

Table 1 Effects of Noopept (NP) on the levels of lipid peroxidation (MDA), reduced glutathione (R-GSH) levels, glutathione peroxidase (GSHPx), and antioxidant vitamin in the brain, erythrocyte, liver, kidney, and plasma in the diabetes (STZ)-induced rats (mean ± SD)

	Values	Control (n = 9)	NP (n = 9)	STZ (n = 9)	STZ + NP (n = 9)
MDA (μM/g pr)	Brain	12.46 ± 1.09	11.84 ± 0.58	14.38 ± 1.38[a]	12.56 ± 1.41[b]
	Erythrocyte	16.90 ± 1.48	16.40 ± 0.88	19.50 ± 1.87[a]	17.40 ± 1.36[b]
	Kidney	14.50 ± 1.05	13.20 ± 0.90	17.40 ± 1.26[a]	14.80 ± 1.45[b]
	Liver	19.50 ± 1.46	18.50 ± 1.24	25.90 ± 1.71[a]	20.90 ± 1.91[b]
R-GSH (μM/g pr)	Brain	10.97 ± 0.39	11.43 ± 0.43	9.34 ± 0.25[a]	10.63 ± 0.83[b]
	Erythrocyte	18.80 ± 1.08	19.10 ± 0.81	16.60 ± 1.50[a]	18.00 ± 0.47[b]
	Kidney	11.60 ± 1.00	11.80 ± 0.42	9.88 ± 0.69[a]	11.30 ± 1.16[b]
	Liver	17.60 ± 1.77	18.50 ± 1.27	15.50 ± 1.26[a]	17.30 ± 0.59[b]
GSHPx (μM/g pr)	Brain	21.20 ± 1.90	22.40 ± 1.42	16.60 ± 2.38[a]	20.50 ± 1.12[b]
	Erythrocyte	27.40 ± 1.27	28.20 ± 1.86	21.00 ± 2.47[a]	25.60 ± 1.92[b]
	Kidney	22.50 ± 1.62	23.20 ± 1.15	17.00 ± 1.39[a]	21.90 ± 0.88[b]
	Liver	26.31 ± 0.95	27.43 ± 1.17	22.78 ± 1.79[a]	26.44 ± 2.48[b]
Retinol (μM/g tiss)	Brain	3.66 ± 0.38	3.61 ± 0.33	3.55 ± 0.37	3.63 ± 0.33
	Kidney	3.81 ± 0.68	3.96 ± 0.45	3.78 ± 0.54	3.91 ± 0.36
	Liver	19.77 ± 0.88	20.40 ± 0.79	19.10 ± 0.45	19.25 ± 0.58
	Plasma (μM/l)	3.02 ± 0.45	3.07 ± 0.35	3.09 ± 0.23	3.09 ± 0.36
α-Tocop (μM/g tiss)	Brain	19.50 ± 0.70	20.10 ± 0.17	15.80 ± 1.59[a]	18.70 ± 1.24[b]
	Kidney	16.90 ± 1.20	17.30 ± 1.51	13.20 ± 1.44[a]	16.80 ± 1.30[b]
	Liver	28.70 ± 1.24	29.70 ± 1.70	23.60 ± 1.45[a]	27.90 ± 1.90[b]
	Plasma (μM/l)	24.54 ± 1.61	26.30 ± 1.09	19.86 ± 1.14[a]	23.70 ± 1.05[b]
β-Car (μM/g tiss)	Brain	1.30 ± 0.16	1.27 ± 0.24	1.00 ± 0.07[a]	1.26 ± 0.19[b]
	Kidney	1.50 ± 0.16	1.70 ± 0.25	1.29 ± 0.10[a]	1.50 ± 0.14[b]
	Liver	2.30 ± 0.36	2.48 ± 0.28	1.89 ± 0.34[a]	2.27 ± 0.38[b]

[a] $p \leq 0.05$ *vs* control (Ctr) and NP groups

[b] $p \leq 0.05$ *vs* STZ group

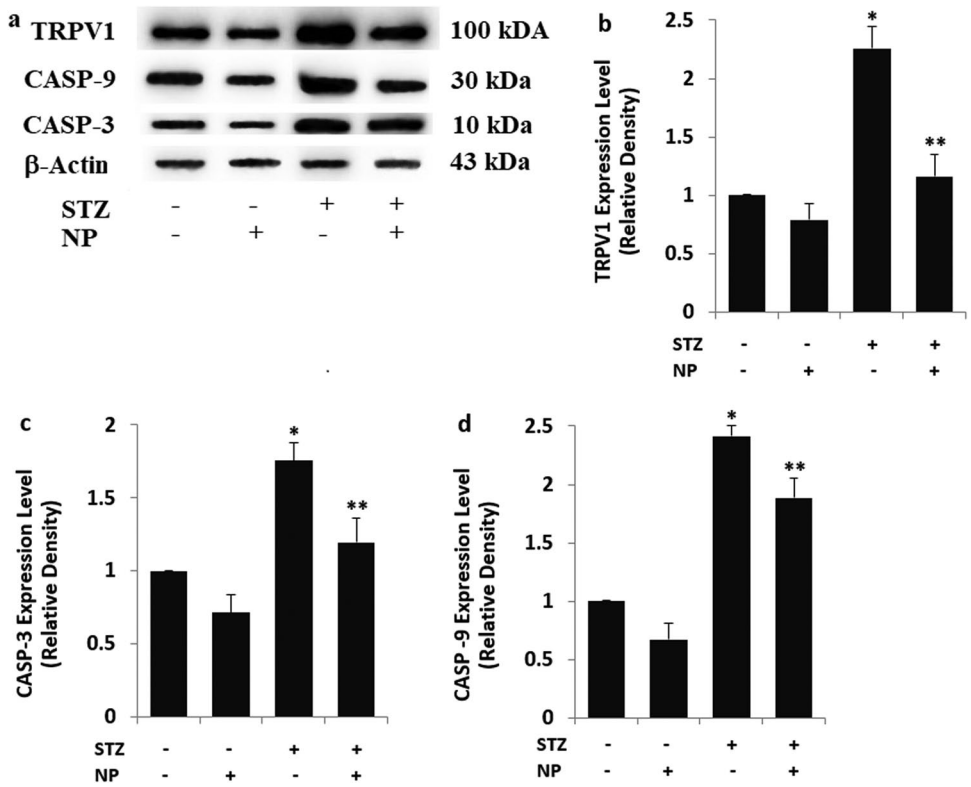

Fig. 10 STZ-mediated the increase of TRPV1 and apoptotic mediator expression levels were attenuated by the treatment of NP. (Mean ± SD and $n = 3$). **a** The Western blot imaging bands**. b, c,** and **d** represent the mean values of TRPV1, CASP-3, and CASP-9 in the DRGs, respectively. ($^{*}p \leq 0.05$ *vs* the groups of control (Ctr) and NP. $^{**}p \leq 0.05$ *vs* the group of STZ)

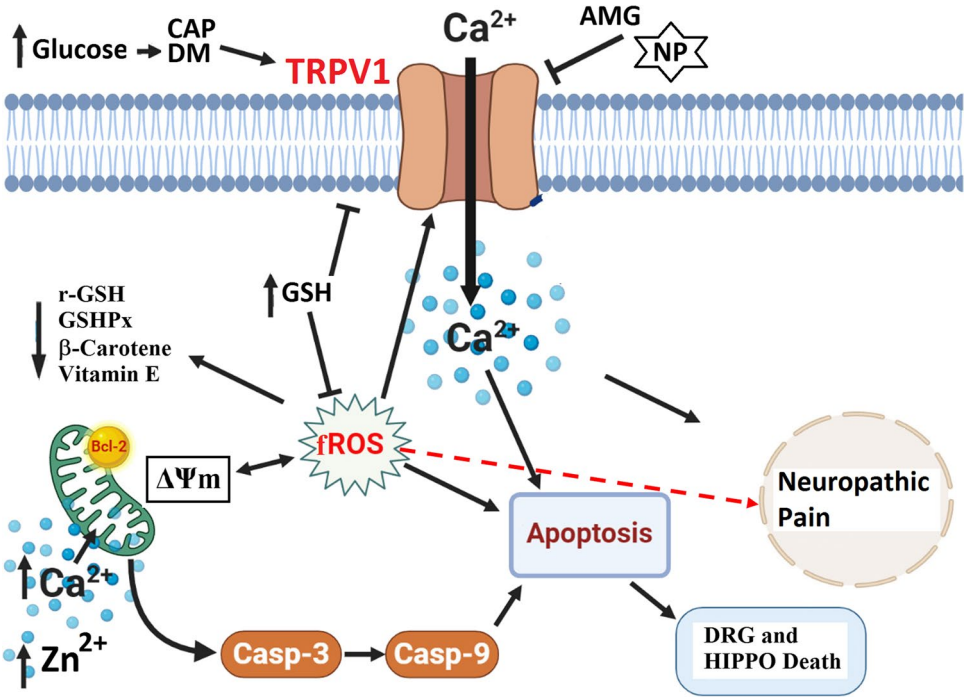

Fig. 11 The possible protective action of noopept (NP) on the molecular pathways of oxidative stress, apoptosis, and neuropathic pain via the inhibition of TRPV1 in dorsal root ganglion (DRG) and hippocampus (HIPPO) of rats with diabetes. The well-known agonist and antagonist of TRPV1 are capsaicin (CAP) and AMG9810 (AMG). The increase of free Ca^{2+} and Zn^{2+} in the cytosol of DRG and HIPPO via the activation of TRPV1 causes the increase of mitochondrial membrane depolarization (ΔΨm). In turn, the increase of ΔΨm causes the excessive generation of free reactive oxygen species (fROS), and the decrease of cytosolic glutathione (GSH), reduced glutathione (R-GSH), glutathione peroxidase (GSHPx), β-carotene, and vitamin E level. The fROS and TRPV1 activation mediate excessive Ca^{2+} influx cause apoptosis and cell death via the activations of caspase pathways such as caspase -3 and caspase -9 in the DRG and HIPPO of rats with diabetes mellitus (DM). The excessive glucose in the DM causes the excessive generation of fROS and TRPV1 activation. The neuropathic, oxidant, and apoptosis actions of DM are modulated by the treatment of NP. (↑) Increase. (↓) Decrease

were reported in the brain, erythrocyte, kidney, liver, and plasma. The protective role of NP has been shown to act as an antidiabetic by probable different mechanisms, including neuroprotective and antioxidant activities [24, 25]. In the current study, the STZ-induced decrease of vitamin E and β-carotene in the brain, erythrocyte, kidney, liver, and plasma were upregulated by the treatment of NP. The fROS scavenger action of NP induced the increase of vitamin E and β-carotene in the tissues.

In this research, NP has been determined to, has neuroprotective effect on HIPPO and DRGs, decrease neuropathic pain, act on TRPV1 channels and potentially regulate diabetes-induced impairment of intracellular Ca^{2+} homeostasis. As the result, NP-mediated protective effects against STZ-induced adverse peripheral and HIPPO oxidative neurotoxicity and peripheral pain. These effects might attribute to the potent antioxidant property of NP, and these findings specify NP to be a candidate agent that may be effective in the prevention and management of diabetes and diabetic neuropathy.

Acknowledgements The authors wish thanks to technician Fatih Şahin (BSN Health, Analyses, Innovation, Consultancy, Organization, Agriculture, and Industry Ltd., Isparta, Turkey) for helping the patch-clamp analyses.

Authors' Contribution Dr. Duzova, Dr. Gurbuz and Dr. Akatlı reviewed the current literature, and designed the project. Dr. Cig performed animal care and experiments. Dr. Gurbuz and Dr. Cig performed the rat experimental processes. Dr. Naziroglu performed and analyzed patch clamp, Western blot, and spectrofluorometer tests. Dr. Duzova and Dr. Naziroglu conceptualized this perspective piece, reviewed and revised the manuscript. All authors approved the final manuscript as submitted.

Funding This research was supported by the Inonu University, BAPSIS (Project number: TCD-2019–624). Coordinator of the project was Dr. Duzova.

Availability of Data and Materials The row data are available from the Professor M. Nazıroğlu on reasonable request. The preparation of the graphics in the manuscript were performed by Professor M. Nazıroğlu.

Declarations

Ethics Approval This article does not contain any studies with human participants performed by any of the authors. This study was carried out with approvals of Inonu University Medical School Experimental Animals Ethics Committee (2017/A-13) and Experimental Animal Research Center of SDU (Permit Numbers: 2019–06-03. Date 25.04.2019). The authors have no ethical conflicts to disclose.

Consent to Participate Dr. Duzova, Dr. Gurbuz and Dr. Akatlı reviewed the current literature, and designed the project. Dr. Cig performed animal care and experiments. Dr. Gurbuz and Dr. Cig performed the experimental process. Dr. Naziroglu performed and analyzed patch clamp, Western blot, and spectrofluorometer tests. Dr. Duzova, Dr. Naziroglu, and Dr. Gurbuz conceptualized this perspective piece, reviewed and revised the manuscript. All authors approved the final manuscript as submitted.

Consent for Publication Last version of the manuscript was approved by the authors before the submission.

Conflict of Interest The authors have no conflicts of interest to declare.

Research involving Human Participants and/or Animals Human and human samples were not used in the present study. Rat and rat tissue samples were used in the current study.

References

1. Fathizadeh H, Milajerdi A, Reiner Ž et al (2020) The effects of L-carnitine supplementation on indicators of inflammation and oxidative stress: a systematic review and meta-analysis of randomized controlled trials. J Diabetes Metab Disord 19(2):1879–1894. https://doi.org/10.1007/s40200-020-00627-9
2. Naranjo C, Ortega-Jiménez P, Del Reguero L, Moratalla G, Failde I (2020) Relationship between diabetic neuropathic pain and comorbidity. Their impact on pain intensity, diabetes complications and quality of life in patients with type-2 diabetes mellitus. Diabetes Res Clin Pract 165:108236. https://doi.org/10.1016/j.diabres.2020.108236
3. Basu P, Basu A (2020) In vitro and in vivo effects of flavonoids on peripheral neuropathic pain. Molecules 25(5):1171. https://doi.org/10.3390/molecules25051171
4. Sima AA, Zhang W (2014) Mechanisms of diabetic neuropathy: axon dysfunction. Handb Clin Neurol 126:429–442. https://doi.org/10.1016/B978-0-444-53480-4.00031-X
5. Liu W, Liang XC, Shi Y (2020) Effects of hirudin on high glucose-induced oxidative stress and inflammatory pathway in rat dorsal root ganglion neurons. Chin J Integr Med 26(3):197–204. https://doi.org/10.1007/s11655-019-2712-8
6. Huerta-Cervantes M, Peña-Montes DJ, Montoya-Pérez R et al (2020) Gestational diabetes triggers oxidative stress in hippocampus and cerebral cortex and cognitive behavior modifications in rat offspring: Age- and sex-dependent effects. Nutrients 12(2):376. https://doi.org/10.3390/nu12020376
7. Carrasco C, Naziroğlu M, Rodríguez AB, Pariente JA (2018) Neuropathic Pain: Delving into the oxidative origin and the possible implication of transient receptor potential channels. Front Physiol 9:95. https://doi.org/10.3389/fphys.2018.00095
8. Sözbir E, Nazıroğlu M (2016) Diabetes enhances oxidative stress-induced TRPM2 channel activity and its control by N-acetylcysteine in rat dorsal root ganglion and brain. Metab Brain Dis 31(2):385–393. https://doi.org/10.1007/s11011-015-9769-7
9. Özdemir ÜS, Nazıroğlu M, Şenol N, Ghazizadeh V (2016) Hypericum perforatum attenuates spinal cord injury-induced oxidative stress and apoptosis in the dorsal root ganglion of rats: Involvement of TRPM2 and TRPV1 channels. Mol Neurobiol 53(6):3540–3551. https://doi.org/10.1007/s12035-015-9292-1
10. Garcilazo C, Cavallasca JA, Musuruana JL (2010) Shoulder manifestations of diabetes mellitus. Curr Diabetes Rev 6(5):334–340. https://doi.org/10.2174/157339910793360824
11. Knezevic NN, Jovanovic F, Candido KD, Knezevic I (2020) Oral pharmacotherapeutics for the management of peripheral neuropathic pain conditions - a review of clinical trials. Expert Opin Pharmacother 21(18):2231–2248. https://doi.org/10.1080/14656566.2020.1801635
12. Düll MM, Riegel K, Tappenbeck J, Ries V, Strupf M, Fleming T, Sauer SK, Namer B (2019) Methylglyoxal causes pain and hyperalgesia in human through C-fiber activation. Pain 160(11):2497–2507. https://doi.org/10.1097/j.pain.0000000000001644
13. Kahya MC, Nazıroğlu M, Övey İS (2017) Modulation of diabetes-induced oxidative stress, apoptosis, and Ca(2+) entry through TRPM2 and TRPV1 channels in dorsal root ganglion and hippocampus of diabetic rats by melatonin and selenium. Mol Neurobiol 54(3):2345–2360. https://doi.org/10.1007/s12035-016-9727-3
14. Nazıroğlu M, Öz A, Yıldızhan K (2020) Selenium and neurological diseases: Focus on peripheral pain and TRP channels. Curr Neuropharmacol 18(6):501–517. https://doi.org/10.2174/1570159X18666200106152631
15. Nazıroğlu M, Dikici DM, Dursun S (2012) Role of oxidative stress and Ca^{2+} signaling on molecular pathways of neuropathic pain in diabetes: focus on TRP channels. Neurochem Res 37(10):2065–2075. https://doi.org/10.1007/s11064-012-0850-x
16. Nazıroğlu M (2012) Molecular role of catalase on oxidative stress-induced Ca(2+) signaling and TRP cation channel activation in nervous system. J Recept Signal Transduct Res 32(3):134–141. https://doi.org/10.3109/10799893.2012.672994
17. Caterina MJ, Schumacher MA, Tominaga M, Rosen TA, Levine JD, Julius D (1997) The capsaicin receptor: a heat-activated ion channel in the pain pathway. Nature 389(6653):816–824
18. Ibi M, Matsuno K, Shiba D et al (2008) Reactive oxygen species derived from NOX1/NADPH oxidase enhance inflammatory pain. J Neurosci 28(38):9486–9494
19. Gavva NR, Tamir R, Qu Y et al (2005) AMG 9810 [(E)-3-(4-t-butylphenyl)-N-(2,3-dihydrobenzo[b][1,4] dioxin-6-yl)acrylamide], a novel vanilloid receptor 1 (TRPV1) antagonist with antihyperalgesic properties. J Pharmacol Exp Ther 313(1):474–484. https://doi.org/10.1124/jpet.104.079855
20. Yu L, Yang F, Luo H et al (2008) The role of TRPV1 in different subtypes of dorsal root ganglion neurons in rat chronic inflammatory nociception induced by complete Freund's adjuvant. Mol Pain 4:61. https://doi.org/10.1186/1744-8069-4-61
21. Hakimizadeh E, Oryan S, Hajizadeh Moghaddam A, Shamsizadeh A, Roohbakhsh A (2012) Endocannabinoid system and TRPV1 receptors in the dorsal hippocampus of the rats modulate anxiety-like behaviors. Iran J Basic Med Sci 15(3):795–802
22. Chukyo A, Chiba T, Kambe T et al (2018) Oxaliplatin-induced changes in expression of transient receptor potential channels in the dorsal root ganglion as a neuropathic mechanism for cold hypersensitivity. Neuropeptides 67:95–101. https://doi.org/10.1016/j.npep.2017.12.002

23. Tóth A, Boczán J, Kedei N et al (2005) Expression and distribution of vanilloid receptor 1 (TRPV1) in the adult rat brain. Brain Res Mol Brain Res 135(1–2):162–168. https://doi.org/10.1016/j.molbrainres.2004.12.003
24. Kolbaev SN, Aleksandrova OP, Sharonova IN, Skrebitsky VG (2018) Effect of noopept on dynamics of intracellular calcium in neurons of cultured rat hippocampal slices. Bull Exp Biol Med 164(3):330–333. https://doi.org/10.1007/s10517-018-3983-3
25. Gürbüz P, Düzova H, Yildiz A et al (2019) Effects of noopept on cognitive functions and pubertal process in rats with diabetes. Life Sci 233:116698. https://doi.org/10.1016/j.lfs.2019.116698
26. Pelsman A, Hoyo-Vadillo C, Gudasheva TA, Seredenin SB, Ostrovskaya RU, Busciglio J (2003) GVS-111 prevents oxidative damage and apoptosis in normal and Down's syndrome human cortical neurons. Int J Dev Neurosci 21(3):117–124. https://doi.org/10.1016/s0736-5748(03)00031-5
27. Wilms W, Woźniak-Karczewska M, Corvini PF, Chrzanowski Ł (2019) Nootropic drugs: Methylphenidate, modafinil and piracetam - Population use trends, occurrence in the environment, ecotoxicity and removal methods - A review. Chemosphere 233:771–785. https://doi.org/10.1016/j.chemosphere.2019.06.016
28. Nistor M, Behringer W, Schmidt M, Schiffner R (2017) A Systematic review of neuroprotective strategies during hypovolemia and hemorrhagic shock. Int J Mol Sci 18(11):2247. https://doi.org/10.3390/ijms18112247
29. Lutsenko VK, Vukolova MN, Gudasheva TA (2003) Cyclopropyl glycine and proline-containing preparation noopept evoke two types of membrane potential responses in synaptoneurosomes. Bull Exp Biol Med 135(6):559–562. https://doi.org/10.1023/a:1025425218023
30. Bukanova JV, Solntseva EI, Skrebitsky VG (2002) Selective suppression of the slow-inactivating potassium currents by nootropics in molluscan neurons. Int J Neuropsychopharmacol 5(3):229–237. https://doi.org/10.1017/S1461145702002997
31. Solntseva EI, Bukanova JV, Ostrovskaya RU, Gudasheva TA, Voronina TA, Skrebitsky VG (1997) The effects of piracetam and its novel peptide analogue GVS-111 on neuronal voltage-gated calcium and potassium channels. Gen Pharmacol 29(1):85–89. https://doi.org/10.1016/s0306-3623(96)00529-0
32. Andreeva NA, Stel'mashuk EV, Isaev NK, Ostrovskaya RU, Gudasheva TA, Viktorov IV (2000) Neuroprotective properties of nootropic dipeptide GVS-111 in in vitro oxygen-glucose deprivation, glutamate toxicity and oxidative stress. Bull Exp Biol Med 130(10):969–972
33. Ostrovskaya RU, Vakhitova YV, Kuzmina USh et al (2014) Neuroprotective effect of novel cognitive enhancer noopept on AD-related cellular model involves the attenuation of apoptosis and tau hyperphosphorylation. J Biomed Sci 21(1):74. https://doi.org/10.1186/s12929-014-0074-2
34. Ostrovskaya RU, Ozerova IV, Gudascheva TA, Kapitsa IG, Ivanova EA, Voronina TA, Seredenin SB (2013) Efficiency of noopept in streptozotocin-induced diabetes in rats. Bull Exp Biol Med 154(3):334–338. https://doi.org/10.1007/s10517-013-1944-4
35. Ostrovskaya RU, Zolotov NN, Ozerova IV, Ivanova EA, Kapitsa IG, Taraban KV, Michunskaya AM, Voronina TA et al (2014) Noopept normalizes parameters of the incretin system in rats with experimental diabetes. Bull Exp Biol Med 157(3):344–349. https://doi.org/10.1007/s10517-014-2562-5
36. Özkaya D, Nazıroğlu M, Armağan A et al (2011) Dietary vitamin C and E modulates oxidative stress induced-kidney and lens injury in diabetic aged male rats through modulating glucose homeostasis and antioxidant systems. Cell Biochem Funct 29(4):287–293. https://doi.org/10.1002/cbf.1749
37. Yüksel E, Nazıroğlu M, Şahin M, Çiğ B (2017) Involvement of TRPM2 and TRPV1 channels on hyperalgesia, apoptosis and oxidative stress in rat fibromyalgia model: Protective role of selenium. Sci Rep 7(1):17543. https://doi.org/10.1038/s41598-017-17715-1
38. Mohammadi-Farani A, Ghazi-Khansari M, Sahebgharani M (2014) Glucose concentration in culture medium affects mRNA expression of TRPV1 and CB1 receptors and changes capsaicin toxicity in PC12 cells. Iran J Basic Med Sci 17(9):673–378
39 Joshi DC, Bakowska JC (2011) Determination of mitochondrial membrane potential and reactive oxygen species in live rat cortical neurons. J Vis Exp 51:2704. https://doi.org/10.3791/2704
40. Keil VC, Funke F, Zeug A, Schild D, Müller M (2011) Ratiometric high-resolution imaging of JC-1 fluorescence reveals the subcellular heterogeneity of astrocytic mitochondria. Pflugers Arch 462:693–708. https://doi.org/10.1007/s00424-011-1012-8
41. Yıldızhan K, Nazıroğlu M (2020) Glutathione depletion and parkinsonian neurotoxin MPP^+-induced TRPM2 channel activation play central roles in oxidative cytotoxicity and inflammation in microglia. Mol Neurobiol 57(8):3508–3525. https://doi.org/10.1007/s12035-020-01974-7
42. Placer ZA, Cushman L, Johnson BC (1966) Estimation of products of lipid peroxidation (malonyl dialdehyde) in biological fluids. Anal Biochem 16:359–364
43. Sedlak J, Lindsay RHC (1968) Estimation of total, protein bound and non-protein sulfhydryl groups in tissue with Ellmann' s reagent. Anal Biochem 25:192–205
44. Lowry OH, Rosebrough NJ, Farr AL, Randall RJ (1951) Protein measurement with the Folin phenol reagent. J Biol Chem 193(1):265–275
45. Lawrence RA, Burk RF (2012) Glutathione peroxidase activity in selenium-deficient rat liver. Biochem Biophys Res Commun 425(3):503–509
46. Desai ID (1980) Vitamin E analysis methods for animal tissues. Methods Enzymol 105:138–147
47. Suzuki J, Katoh N (1990) A simple and cheap method for measuring vitamin A in cattle using only a spectrophotometer. Jpn J Vet Sci 52:1282–1284
48. Racay P, Tatarkova Z, Chomova M, Hatok J, Kaplan P, Dobrota D (2009) Mitochondrial calcium transport and mitochondrial dysfunction after global brain ischemia in rat hippocampus. Neurochem Res 34(8):1469–1478. https://doi.org/10.1007/s11064-009-9934-7
49. Pinton P, Giorgi C, Siviero R, Zecchini E, Rizzuto R (2008) Calcium and apoptosis: ER-mitochondria Ca2+ transfer in the control of apoptosis. Oncogene 27(50):6407–6418. https://doi.org/10.1038/onc.2008.308
50. Yoon H, Thakur V, Isham D, Fayad M, Chattopadhyay M (2015) Moderate exercise training attenuates inflammatory mediators in DRG of Type 1 diabetic rats. Exp Neurol 267:107–114. https://doi.org/10.1016/j.expneurol.2015.03.006
51. Zhang BY, Zhang YL, Sun Q et al (2020) Alpha-lipoic acid downregulates TRPV1 receptor via NF-κB and attenuates neuropathic pain in rats with diabetes. CNS Neurosci Ther 26(7):762–772. https://doi.org/10.1111/cns.13303
52. Nazıroğlu M (2017) Activation of TRPM2 and TRPV1 channels in dorsal root ganglion by NADPH oxidase and protein kinase C molecular pathways: a Patch clamp study. J Mol Neurosci 61(3):425–435. https://doi.org/10.1007/s12031-017-0882-4
53. Santos CX, Tanaka LY, Wosniak J, Laurindo FR (2009) Mechanisms and implications of reactive oxygen species generation during the unfolded protein response: roles of endoplasmic reticulum oxidoreductases, mitochondrial electron transport, and NADPH oxidase. Antioxid Redox Signal 11(10):2409–24027. https://doi.org/10.1089/ars.2009.2625

54. Sakaguchi R, Mori Y (2020) Transient receptor potential (TRP) channels: Biosensors for redox environmental stimuli and cellular status. Free Radic Biol Med 146:36–44. https://doi.org/10.1016/j.freeradbiomed.2019.10.415
55. Espino J, Bejarano I, Paredes SD, Barriga C, Rodríguez AB, Pariente JA (2011) Protective effect of melatonin against human leukocyte apoptosis induced by intracellular calcium overload: relation with its antioxidant actions. J Pineal Res 51(2):195–206. https://doi.org/10.1111/j.1600-079X.2011.00876.x
56. Halliwell B (2001) Role of free radicals in the neurodegenerative diseases: therapeutic implications for antioxidant treatment. Drugs Aging 18(9):685–716. https://doi.org/10.2165/00002512-200118090-00004